

The iPIC3D code and its applications to 3D magnetic reconnection

Stefano Markidis

High Performance Computing and Visualization Department
KTH Royal Institute of Technology
Stockholm, Sweden



Outline

- iPIC3D code and its algorithm.
- 3 different simulation initial set-up to study different physical problems:
 - 1) Antiparallel Harris equilibrium to study reconnection front instabilities.
 - 2) Harris equilibrium with guide field to study instabilities along the separatrices.
 - 3) Harris current sheet with multiple x-lines to study plasmoid dynamics with and without a guide field.

iPIC3D

- i = implicit (discretization in time of governing equations).
- PIC = Particle-in-Cell method used for simulation of collision-less plasmas.
- 3D = geometry (we have version for 2D geometry).

Open-Source Code

- available at <https://github.com/CmPA/iPic3D>.

The screenshot shows the GitHub repository page for CmPA/iPic3D. The repository is public and has 76 commits, 2 branches, 2 releases, and 3 contributors. The description is "Particle-in-Cell code using the implicit moment method". The latest commit is by murcl3lag0, titled "Performance problems from issue #22", and is dated a month ago. The commit message is "1. Reverting to previous version of EMfields3D.h because the conflict...". The commit is dated 4 months ago. The repository also has a "ConfigFile" and "Documentation" folder, both updated 4 months ago. The right sidebar shows links to Code, Issues (17), Pull Requests (3), Wiki, Pulse, and Graphs.

CmPA/iPic3D

GitHub, Inc. [US] <https://github.com/CmPA/iPic3D>

This repository Search or type a command Explore Gist Blog Help

PUBLIC CmPA / iPic3D Unwatch 7 Star 3 Fork 6

Particle-in-Cell code using the implicit moment method

76 commits 2 branches 2 releases 3 contributors

branch: master iPic3D

Performance problems from issue #22

murcl3lag0 authored a month ago latest commit 034274679b

ConfigFile	1. Reverting to previous version of EMfields3D.h because the conflict...	4 months ago
Documentation	Updated documentation on units	4 months ago

Code

Issues 17

Pull Requests 3

Wiki

Pulse

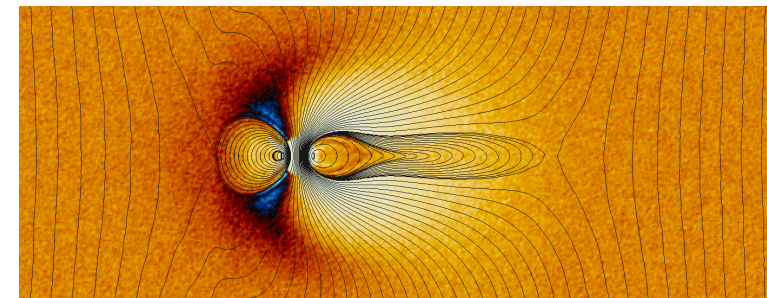
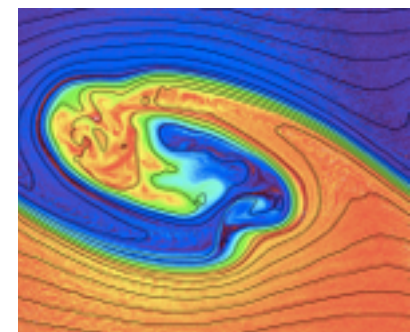
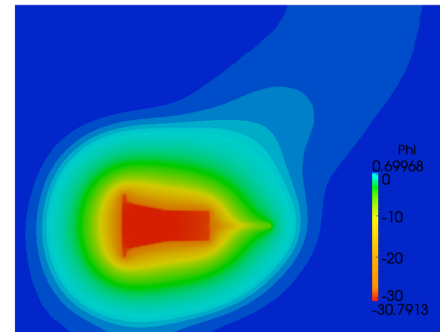
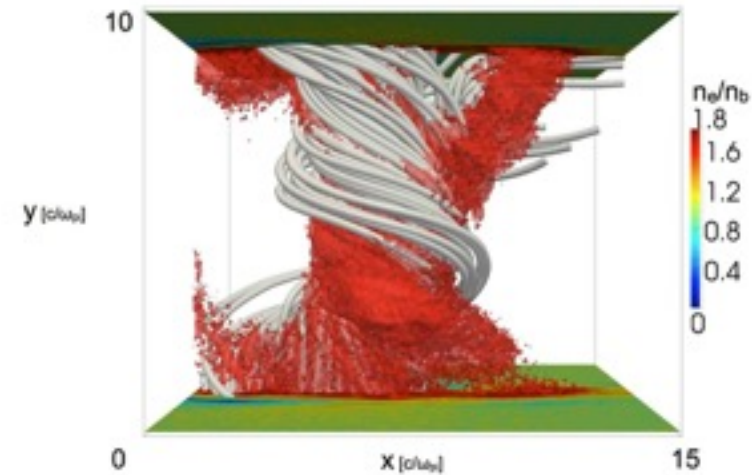
Graphs

Support for iPIC3D development

- iPIC3D development is supported by **European Commission** projects via Exascale Projects:
 - **EPiGRAM** (MPI, PGAS and Communication kernels)
 - **SAGE** (parallel I/O)
 - **INTERTWINE** (interoperability of MPI and other approaches)
 - **Allscale** (task-based models)

Users and Applications

- KTH is developer team (algorithms and parallelization).
- users at KU Leuven, Uppsala University, University of Pisa, University of Colorado.
- Focus on space physics. In particular:
 - magnetic reconnection. Rest of this presentation.
 - Kelvin-Helmholtz instability.
 - Interaction of solar wind with small magnetic dipoles.
 - Spacecraft charging.
- Production runs of iPIC3D provided results for more than 40 publications in physics in the last two years.



Facts About iPIC3D

- C++ code.
- approx 20,000 lines of code.
- parallel with 3D domain decomposition and MPI (C bindings).
- library in use: HDF5.
- post-processing codes in Python, Matlab, IDL.
- OpenMP, OmPSs, OpenACC.
- Hypre/PETSc library.
- Fully implicit

branches main distribution

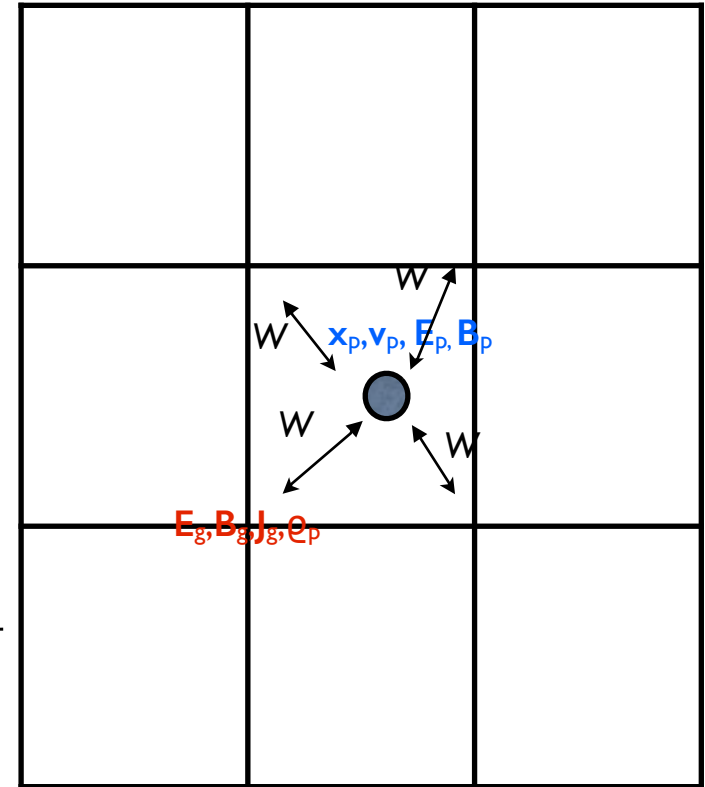
PIC Method Governing Equations

particles

$$\left\{ \begin{array}{l} \frac{d\mathbf{x}_p}{dt} = \mathbf{v}_p \\ \frac{d\mathbf{v}_p}{dt} = \frac{q_s}{m_s} \left(\mathbf{E}_p + \frac{\mathbf{v}_p \times \mathbf{B}_p}{c} \right) \end{array} \right.$$

grid

$$\left\{ \begin{array}{l} \nabla \cdot \mathbf{E} = 4\pi\rho \\ \nabla \cdot \mathbf{B} = 0 \\ 1/c \partial \mathbf{E} / \partial t = \nabla \times \mathbf{B} - 4\pi/c \mathbf{J} \\ 1/c \partial \mathbf{B} / \partial t = -\nabla \times \mathbf{E}, \end{array} \right.$$



coupling
particle-
grid

$$\mathbf{E}_p = \sum_g \mathbf{E}_g W(\mathbf{x} - \mathbf{x}_p) \quad \mathbf{B}_p = \sum_g \mathbf{B}_g W(\mathbf{x} - \mathbf{x}_p)$$

$$\{\rho^n, \mathbf{J}^n, \Pi^n\}_g = \sum_s \sum_p^{N_s} q_s \{1, \mathbf{v}_p^n, \mathbf{v}_p^n \mathbf{v}_p^n\} W(\mathbf{x} - \mathbf{x}_p^n)$$

iPIC3D Uniqueness

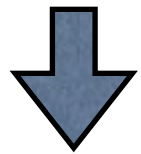
- The vast majority of production PIC codes uses explicit time integration, while **iPIC3D** uses **implicit time integration**.
- The implicit time integration allows us to use time steps and grid spacings that are typically order 10 larger than time steps and grid spacings used in explicit PIC codes. Stability is achieved by numerical damping of the unresolved waves.

Moment-Implicit Method

- iPIC3D uses a semi-implicit PIC method, called “moment-implicit method”. This method makes an implicit formulation of Maxwell’s equation explicit by making a Taylor expansion of the interpolation functions.
- The moment implicit PIC method has been developed by Mason, Brackbill, Forslund at LANL at the beginning of 80s. There are different formulations. The details of the formulation (implicit Maxwell Solver) used in iPIC3D are presented in two reference papers:
 - Markidis, Stefano, and Giovanni Lapenta. "Multi-scale simulations of plasma with iPIC3D." *Mathematics and Computers in Simulation* 80, no. 7 (2010): 1509-1519.
 - Peng, Ivy Bo, et al. "The Formation of a Magnetosphere with Implicit Particle-in-Cell Simulations." *Procedia Computer Science* 51 (2015): 1178-1187.

Implicit Discretization and 2nd order Formulation of Maxwell's Equations

$$\begin{aligned} c\theta\Delta t\nabla \times \mathbf{E}^{n+\theta} + \mathbf{B}^{n+1} - \mathbf{B}^n &= 0, \\ c\theta\Delta t\nabla \times \mathbf{B}^{n+\theta} - (\mathbf{E}^{n+1} - \mathbf{E}^n) &= 4\pi\theta\Delta t\mathbf{J}^{n+1/2} \end{aligned} \quad \mathbf{E}^{n+\theta} = \theta\mathbf{E}^{n+1} + (1-\theta)\mathbf{E}^n$$



Taking the curl of Faraday's law allows to eliminate $\mathbf{B}^{n+\theta}$ and recover an expression for $\mathbf{E}^{n+\theta}$:

$$(c\theta\Delta t)^2\nabla \times \nabla \times \mathbf{E}^{n+\theta} + \mathbf{E}^{n+1} - \mathbf{E}^n = (\theta\Delta t)(c\nabla \times \mathbf{B}^n - 4\pi\mathbf{J}^{n+1/2})$$



Using the vector identity $\nabla \times \nabla = \nabla\nabla \cdot - \nabla^2$, and the Gauss' law $\nabla \cdot \mathbf{E}^{n+\theta} = 4\pi\rho^{n+1/2} = 4\pi(\rho^{n+1} + \rho^n)/2$, we obtain:

$$\mathbf{E}^{n+\theta} - (c\theta\Delta t)^2\nabla^2\mathbf{E}^{n+\theta} = \mathbf{E}^n + c\theta\Delta t(\nabla \times \mathbf{B}^n - 4\pi(\mathbf{J}^{n+1/2} + c\theta\Delta t\nabla\rho^{n+1/2}))$$



$$\frac{\mathbf{B}^{n+1} - \mathbf{B}^n}{\Delta t} = -\nabla \times \mathbf{E}^{n+\theta}$$

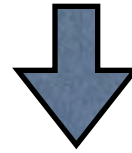
the implicit moment method finds approximate values for these quantities

Moment Implicit PIC method

uses Taylor expansion of interpolation functions W to determine implicit terms

$$W(\mathbf{x} - \mathbf{x}_p^{n+1}) \approx W(\mathbf{x} - \mathbf{x}_p^n) + (\mathbf{x}^n - \mathbf{x}_p^{n+1}) \nabla W(\mathbf{x} - \mathbf{x}_p^n) + \dots$$

$$W(\mathbf{x} - \mathbf{x}_p^{n+1}) \approx W(\mathbf{x} - \mathbf{x}_p^n) - \bar{\mathbf{v}}_p \Delta t \nabla W(\mathbf{x} - \mathbf{x}_p^n) + \dots$$



$$(\mathbf{I} + \chi^n) \cdot \mathbf{E}^{n+1} - (c\Delta t)^2 (\nabla^2 \mathbf{E}^{n+1} + \nabla \nabla \cdot (\chi^n \cdot \mathbf{E}^{n+1})) = \mathbf{E}^n + c\Delta t \left(\nabla \times \mathbf{B}^n - \frac{4\pi}{c} \hat{\mathbf{J}}^n \right) - (c\Delta t)^2 \nabla 4\pi \hat{\rho}^n$$

$$\chi_s = \sum_{n_s} \chi_{s \cdot} \quad , \quad \chi_{s \cdot}^n \equiv \frac{1}{2} (\omega_{ps} \Delta t)^2 R \left(\boldsymbol{\Omega}_s \frac{\Delta t}{2} \right)$$

$$\hat{\rho}^n = \rho^n - \Delta t \nabla \cdot \hat{\mathbf{J}}^n \quad , \quad \hat{\mathbf{J}}^n = \sum_s R \left(\boldsymbol{\Omega}_s \frac{\Delta t}{2} \right) \cdot \left(\mathbf{J}_s^n - \frac{\Delta t}{2} \nabla \Pi_s^n \right)$$

$R(\boldsymbol{\Omega}_s \Delta t/2) \cdot$ is a rotation transformation and it is defined as:

$$\begin{bmatrix} 1 + \left(\Omega_{sx} \frac{\Delta t}{2} \right)^2 & \Omega_{sz} \frac{\Delta t}{2} + \Omega_{sx} \Omega_{sy} \left(\frac{\Delta t}{2} \right)^2 & -\Omega_{sy} \frac{\Delta t}{2} + \Omega_{sx} \Omega_{sz} \left(\frac{\Delta t}{2} \right)^2 \\ -\Omega_{sz} \frac{\Delta t}{2} + \Omega_{sx} \Omega_{sy} \left(\frac{\Delta t}{2} \right)^2 & 1 + \left(\Omega_{sy} \frac{\Delta t}{2} \right)^2 & \Omega_{sx} \frac{\Delta t}{2} + \Omega_{sy} \Omega_{sz} \left(\frac{\Delta t}{2} \right)^2 \\ \Omega_{sy} \frac{\Delta t}{2} + \Omega_{sx} \Omega_{sz} \left(\frac{\Delta t}{2} \right)^2 & -\Omega_{sx} \frac{\Delta t}{2} + \Omega_{sy} \Omega_{sz} \left(\frac{\Delta t}{2} \right)^2 & 1 + \left(\Omega_{sz} \frac{\Delta t}{2} \right)^2 \end{bmatrix}$$

the Maxwell's solver is
now explicit

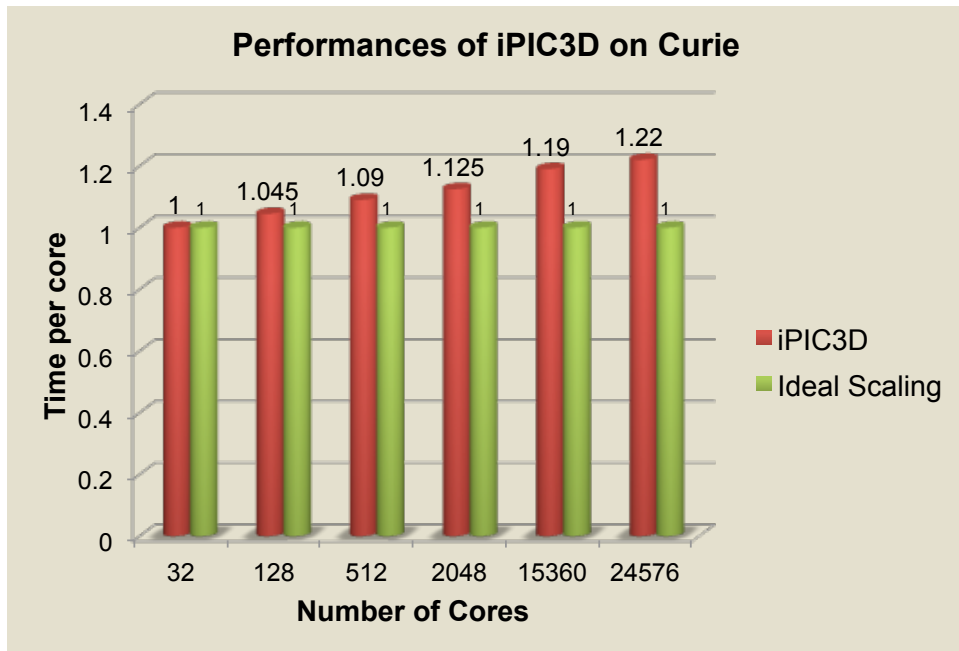
Moment Implicit Method and iPIC3D

$$(\mathbf{I} + \chi^n) \cdot \mathbf{E}^{n+1} - (c\Delta t)^2(\nabla^2 \mathbf{E}^{n+1} + \nabla \nabla \cdot (\chi^n \cdot \mathbf{E}^{n+1})) = \mathbf{E}^n + c\Delta t \left(\nabla \times \mathbf{B}^n - \frac{4\pi}{c} \hat{\mathbf{J}}^n \right) - (c\Delta t)^2 \nabla 4\pi \hat{\rho}^n$$

- is solved with a matrix-free GMRes solver on a uniform Cartesian grid.
- particle mover remains implicit. The equations of motion are solved with a predictor-corrector technique.
- If compared to explicit PIC codes, iPIC3D solves a linear system (instead of a simply update of values) and uses auxiliary variables (both for particles and fields).

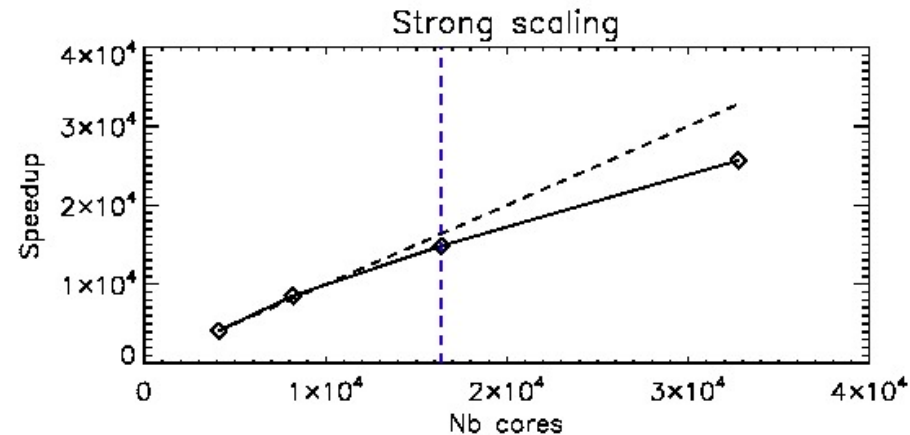
Scaling Tests

Weak Scaling on Curie (Bull)

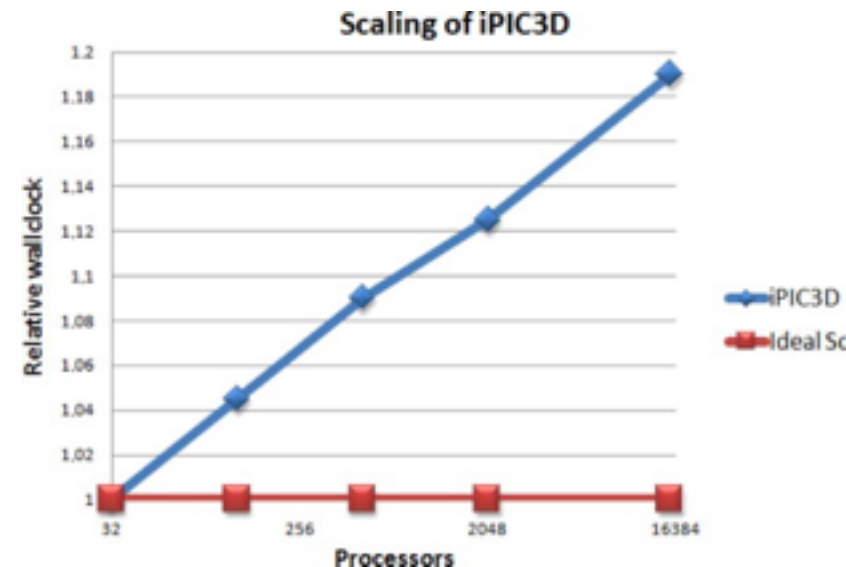


iPIC3D scales on a variety of computing platforms (83% relative parallel efficiency on 20,000 cores).

Strong Scaling on Fermi (BlueGene/Q)




Weak Scaling on Pleiades (SGI)



Fluid-Kinetic Solver in iPIC3D

The fluid-kinetic solver calculates the implicit terms by adding to


$$\mathbf{E}^{n+\theta} - (c\theta\Delta t)^2 \nabla^2 \mathbf{E}^{n+\theta} = \mathbf{E}^n + c\theta\Delta t (\nabla \times \mathbf{B}^n - 4\pi(\mathbf{J}^{n+1/2} + c\theta\Delta t \nabla \rho^{n+1/2}))$$

the first two moment equations

$$\partial \rho_s / \partial t + \nabla \cdot \mathbf{J}_s = 0$$

$$\partial \mathbf{J}_s / \partial t = (q/m)_s (\rho_s \mathbf{E} + (\mathbf{J}_s \times \mathbf{B})/c - \nabla \mathcal{T}_s) \quad \mathcal{T}_s = \mathbf{J}_s \mathbf{J}_s / \rho_s + p_s$$

and use particles to close the fluid equations

$$(\mathcal{T}_s)_g = \sum_p^{N_p} q_s \mathbf{v}_p \mathbf{v}_p W(\mathbf{x}_g - \mathbf{x}_p)$$

Discretized Equations

The fluid-kinetic solver computes the linear system:

$$\begin{aligned}\rho_s^{n+1} - \rho_s^n + \Delta t \nabla \cdot \mathbf{J}_s^{n+1/2} &= 0 \\ \mathbf{J}_s^{n+1} - \mathbf{J}_s^n &= (q/m)_s \Delta t (\rho_s^n \mathbf{E}^{n+\theta} + (\mathbf{J}_s^{n+1/2} \times \mathbf{B}^n)/c - \nabla \mathcal{T}_s^n) \\ \mathbf{E}^{n+\theta} - (c\theta\Delta t)^2 \nabla^2 \mathbf{E}^{n+\theta} &= \mathbf{E}^n + c\theta\Delta t (\nabla \times \mathbf{B}^n - 4\pi(\mathbf{J}^{n+1/2} + c\theta\Delta t \nabla \rho^{n+1/2}))\end{aligned}$$

The stress tensor in momentum equation:

$$\mathbf{J}_s^{n+1} - \mathbf{J}_s^n = \Delta t (q/m)_s (\rho_s^n \mathbf{E}^{n+\theta} + (\mathbf{J}_s^{n+1/2} \times \mathbf{B}^n)/c - \nabla \mathcal{T}_s^n)$$

is calculated at time level n instead of $n+1/2$.

The fluid-kinetic solver can be made “fully implicit” by using the kinetic enslavement technique in the solver.

Results of Fluid-Kinetic Solver

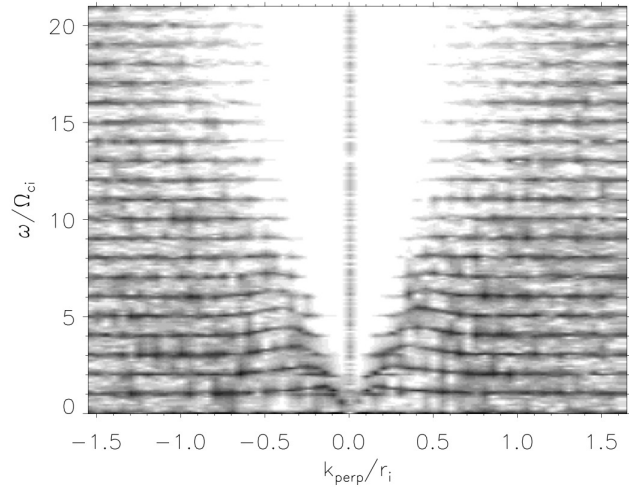


Figure 5: Two-dimensional spectrum of the ion density field. The frequency ω is normalized to the ion cyclotron frequency Ω_{ci} to ease the reading. The perpendicular wavevector k_{perp} is normalized to the ion gyro-radius r_i .

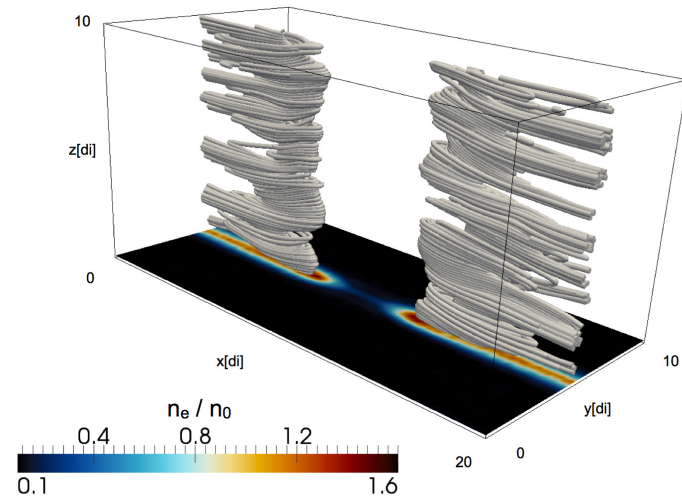


Figure 10: Magnetic field lines and contour plot of the electron density n_e on the plane $z = 0$ at time $\Omega_{ci} t = 11.7$.

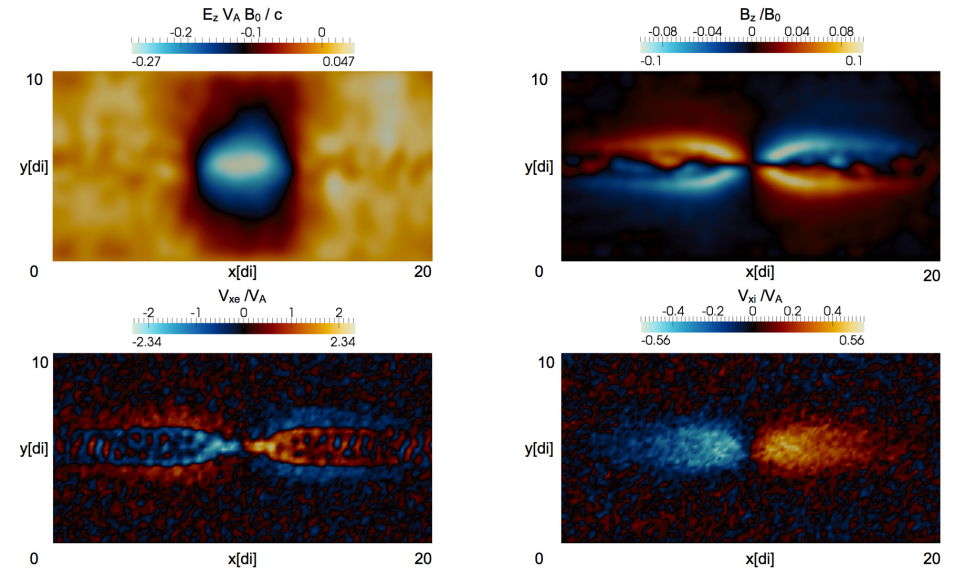


Figure 7: Contour-plots of the different components of electromagnetic fields at time $\Omega_{ci} t = 11.7$ in the two-dimensional magnetic reconnection simulation.

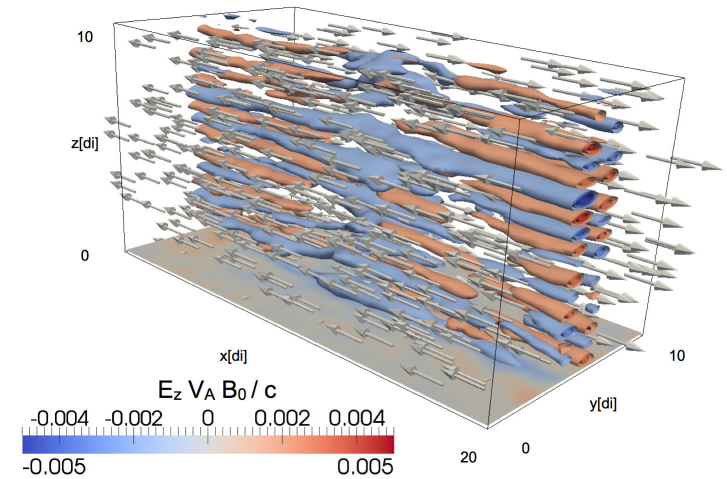
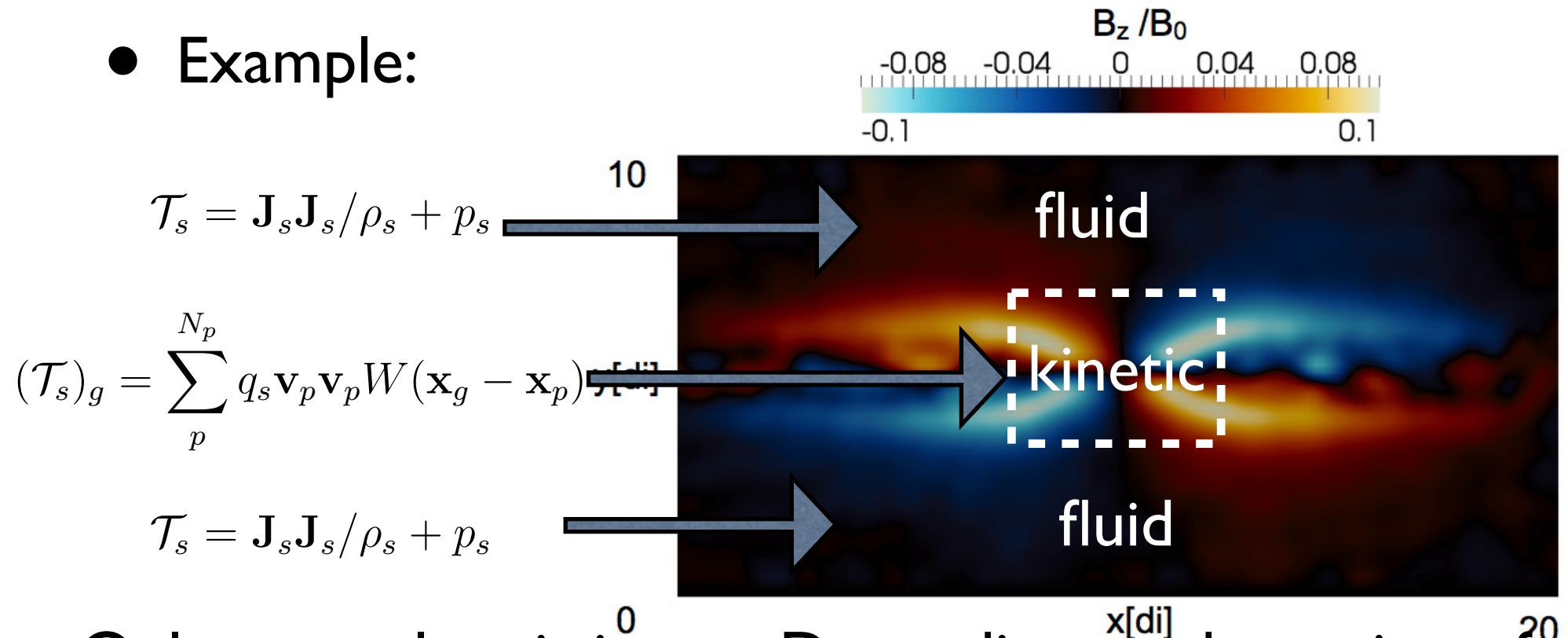


Figure 9: Isosurfaces of the z component of the electric field and quiver plot of the magnetic field \mathbf{B} at time $\Omega_{ci} t = 8.77$. The plot shows features that are present only in three dimensional simulation of magnetic reconnection, such as the presence of the lower-hybrid waves propagating in the z direction.

Towards Fully Integrated Fluid-PIC simulations

- The fluid-kinetic solver is ideal for coupled fluid-PIC simulations in a unified computational framework.

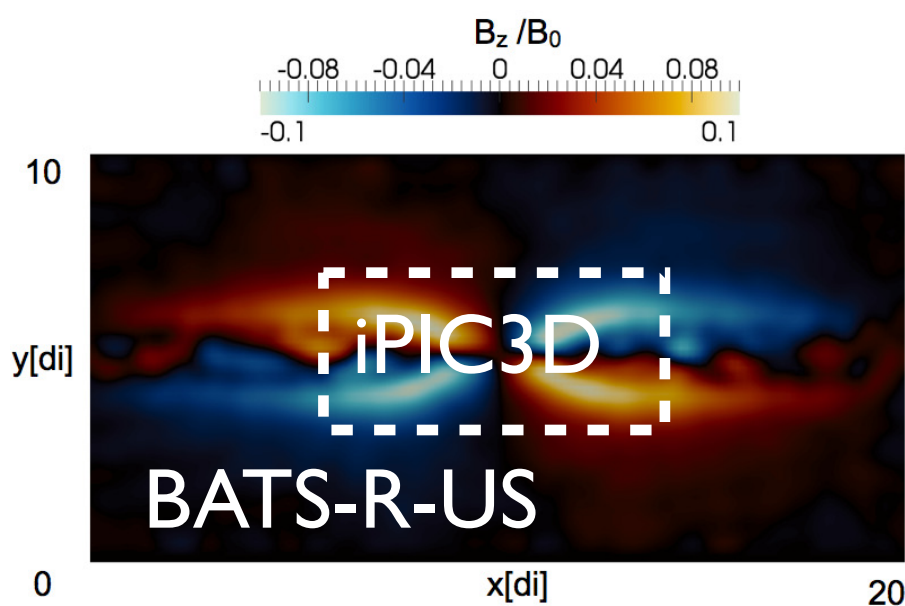
- Example:



Only one solver is in use. Depending on the region of space, the stress tensor can be calculated with particles or with a closure equations.

Coupling of iPIC3D with BATS-R-US and itself

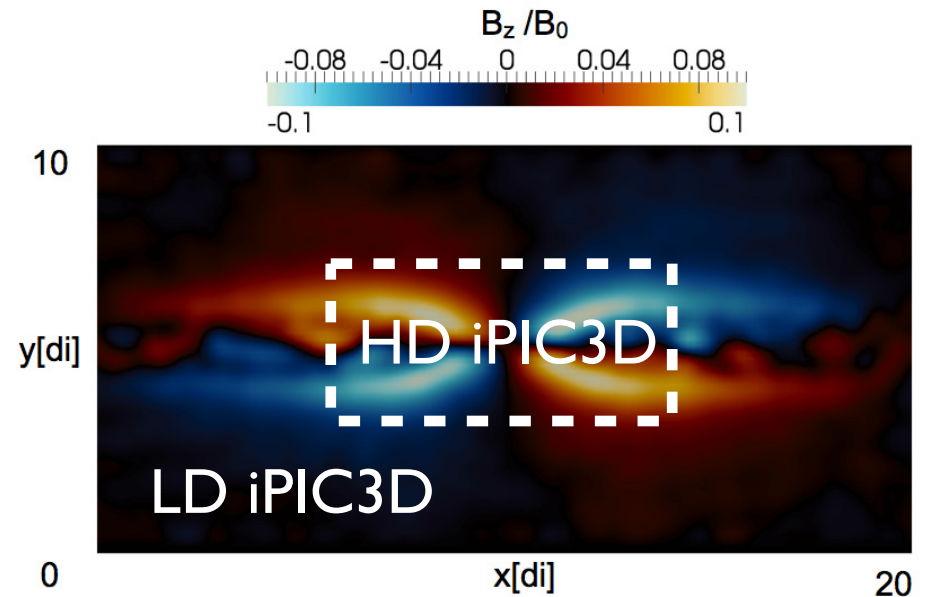
iPIC3D is now available as a **library** that can be dynamically linked with other codes.



Currently, both BATS-R-US and iPIC3D use the same computational resources and are executed sequentially.

Computational cycle

1. BATS-R-US.MHD_step
2. iPIC3D.CouplerIN (to import data from BATS-R-US)
3. iPIC3D.iPIC3D_step
5. iPIC3D.CoupleOUT (to export data to BATS-R-US)



LD = Low Definition (coarse grid)
HD = High Definition (fine grid)
way to provide cheap AMR

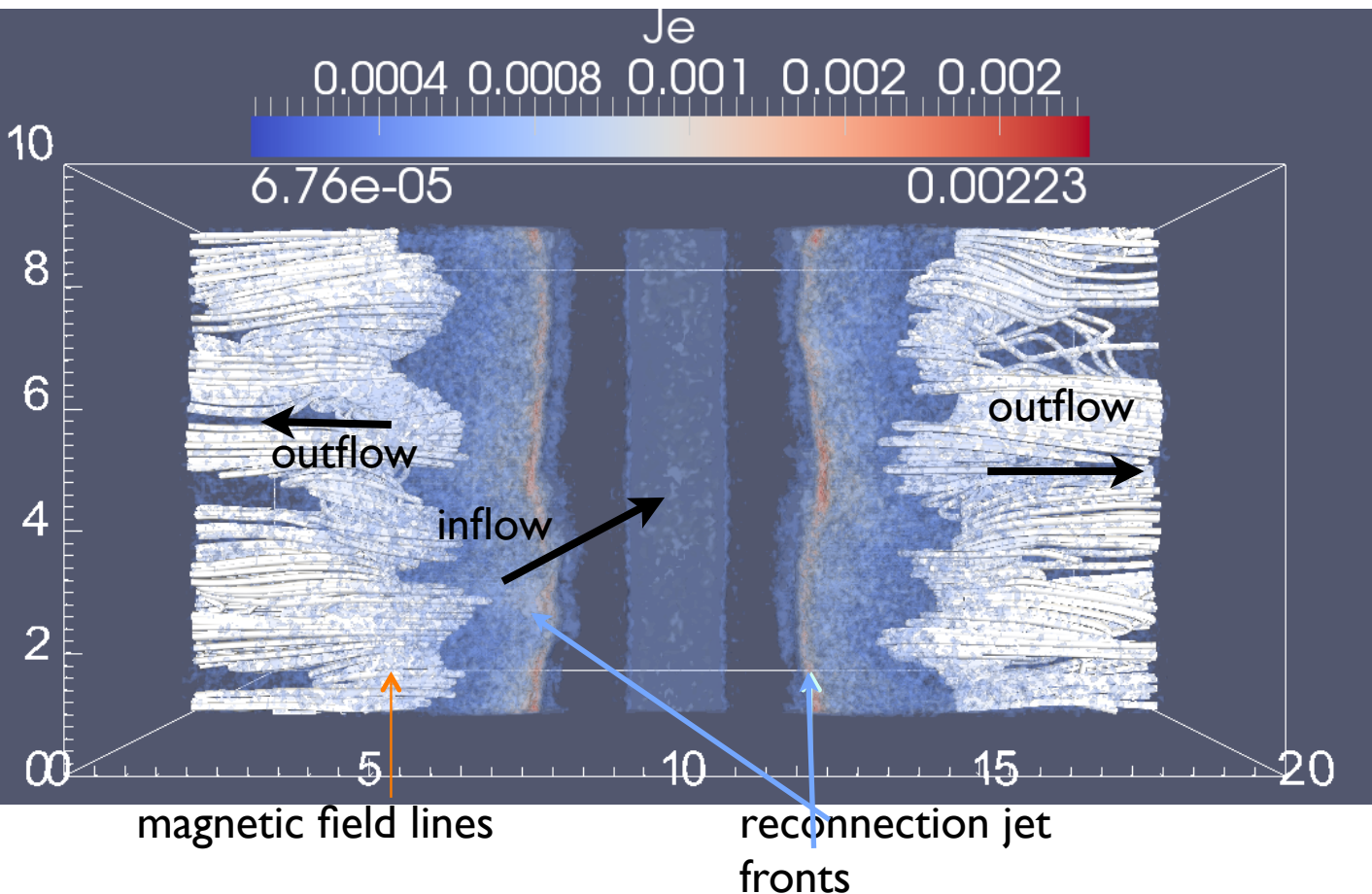
Computational cycle

1. LD.iPIC3D_step
2. HD.iPIC3D_CouplerIN (to import data from LD)
3. HD.iPIC3D_step
5. iPIC3D.CoupleOUT to BATS-R-US (to export data to HD)

I - Harris Equilibrium in Antiparallel B Configuration

- Focus on instabilities affecting the reconnection jet fronts.
- Reference papers:
- Lapenta, Markidis, Goldman, Newman, “Secondary reconnection sites in reconnection-generated flux ropes and reconnection fronts”, Nature Physics (2015).
- G.Lapenta, M. Goldman, D. Newman, S. Markidis, A. Divin, Electromagnetic energy conversion in downstream fronts from three dimensional kinetic reconnection”, POP (2014).
- Vapirev, A. E., G. Lapenta, A. Divin, S. Markidis, P. Henri, M. Goldman, and D. Newman. "Formation of a transient front structure near reconnection point in 3-D PIC simulations." JGR (2013).

Reconnection Jets

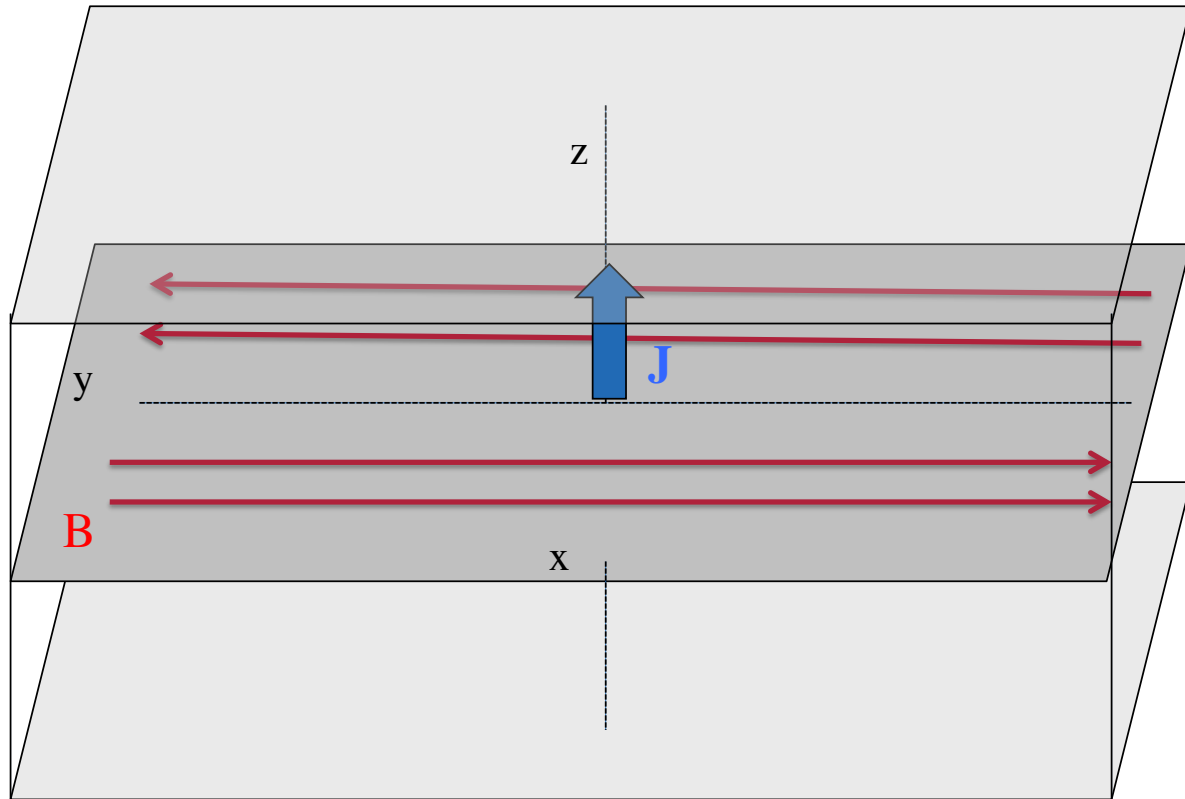


Magnetic reconnection is the topology reorganization of disconnected magnetic regions into a new configuration with concurrent conversion of magnetic energy into plasma kinetic energy.

The magnetic energy is released in form of plasma heating and acceleration: plasma (inflow plasma) drifts toward the region where magnetic reconnection takes place and expelled from it forming the reconnection jets (outflow plasma).

We focus now on studying the instabilities affecting the reconnection jet fronts

Simulation Set-Up



$$B_x(y) = B_0 \tanh\left(\frac{y - L_y/2}{\lambda}\right)$$

$$n(y) = n_0 \cosh^{-2}\left(\frac{y - L_y/2}{\lambda}\right) + n_b$$

$L_x = 40$ di

$L_y = 15$ di

$L_z = 10$ di

$n_{xc} \times n_{yc} \times n_{zc} = 512 \times 192 \times 128$

Periodic BC in x and z

Perfect conductor BC in y

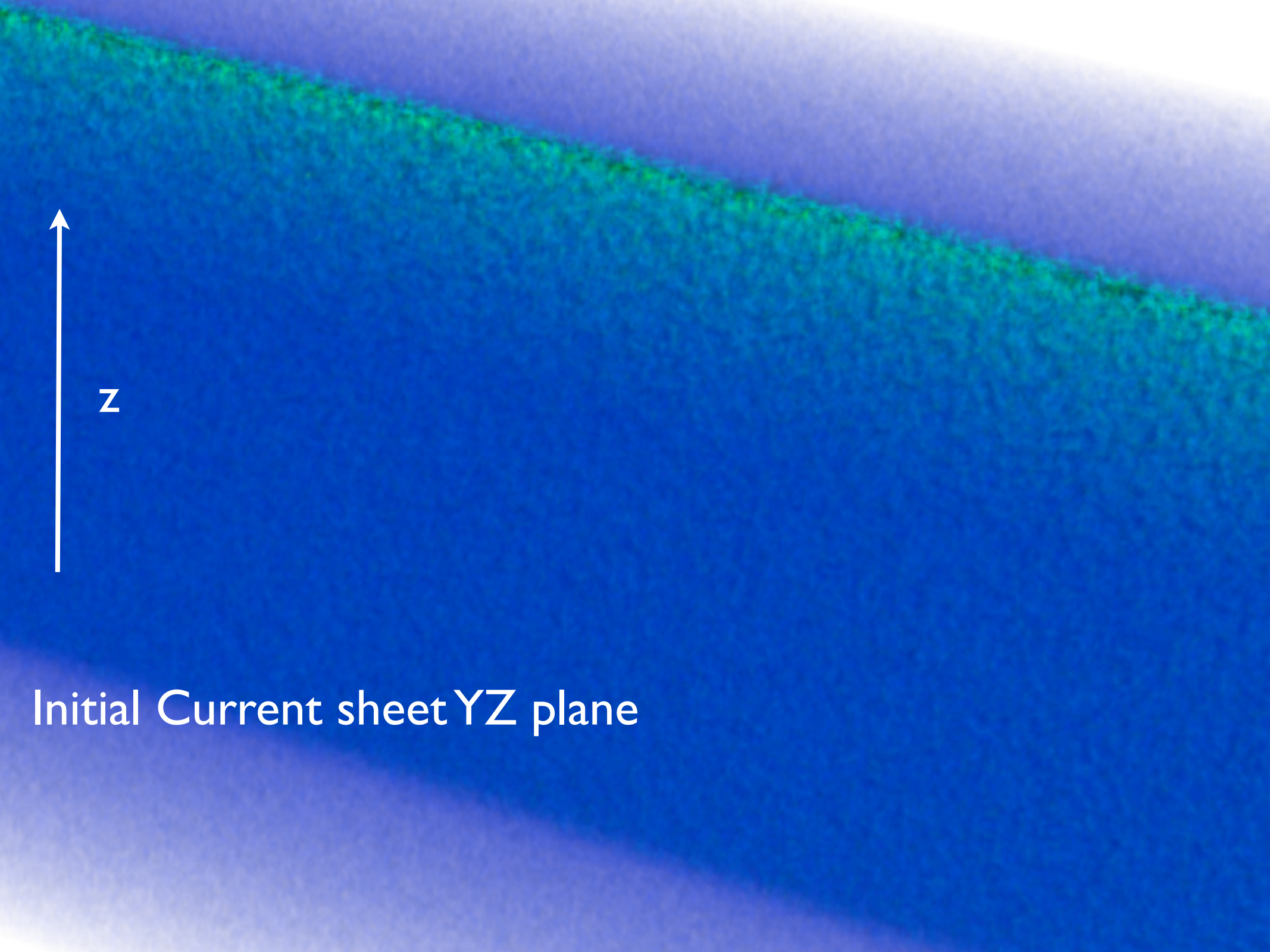
$n_b = 0.1 n_0$

Other parameters are from the GEM challenge

$$\Delta t = 0.125 \omega_{pi}^{-1} \rightarrow \Delta t = 2 \omega_{pe}^{-1}$$

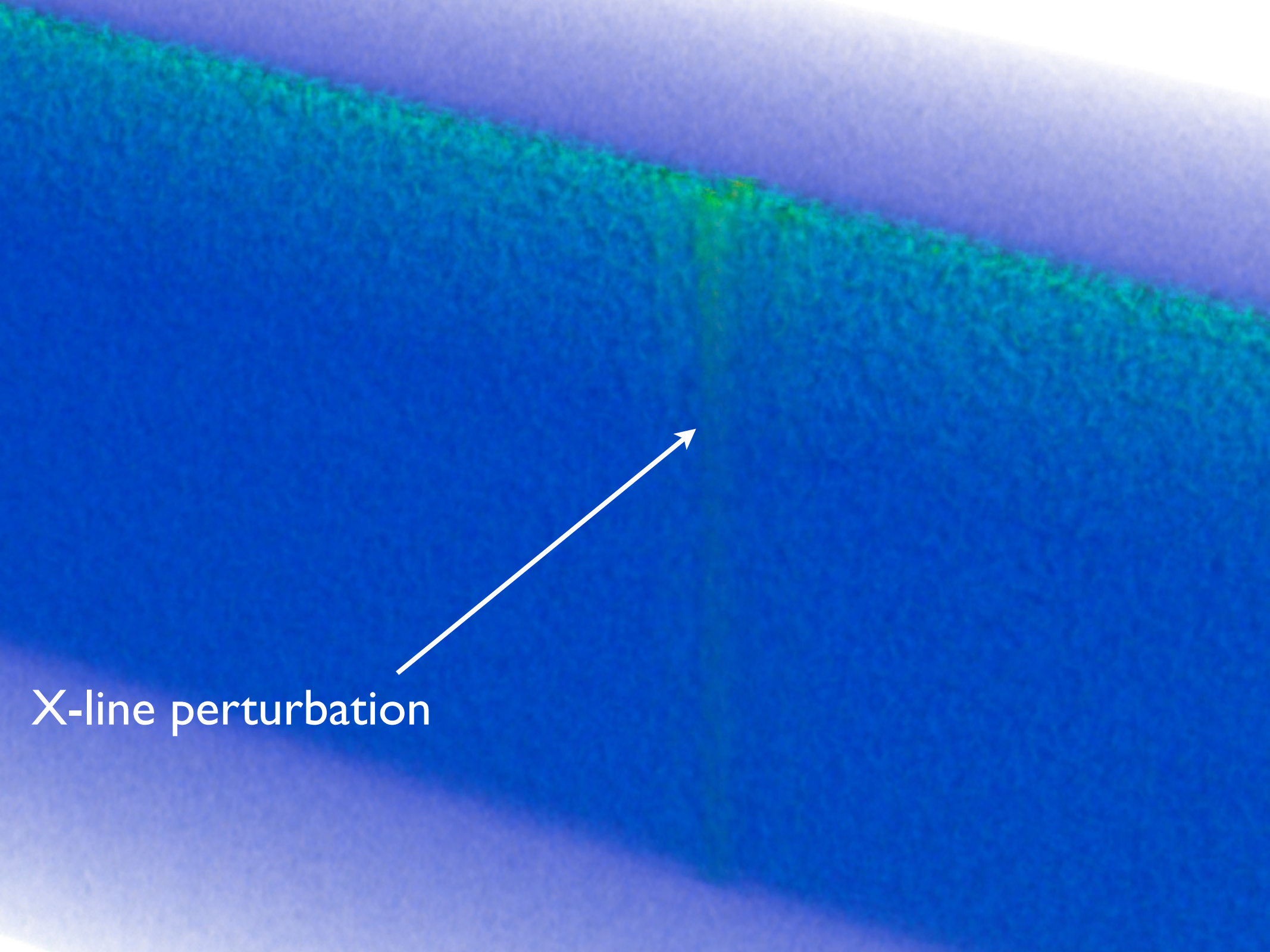
$m_i/m_e = 256$

Initial Perturbation along the dashed line.

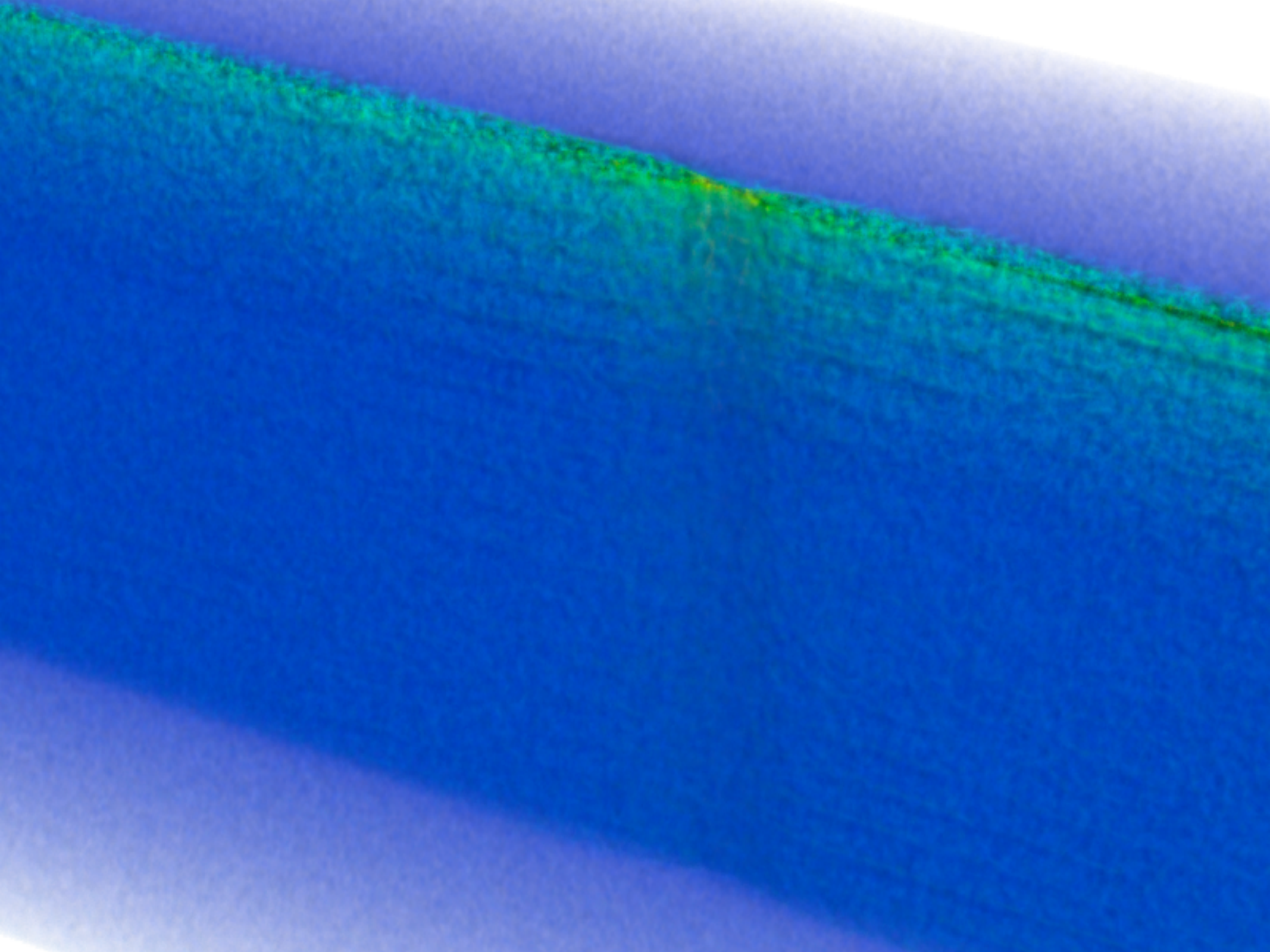


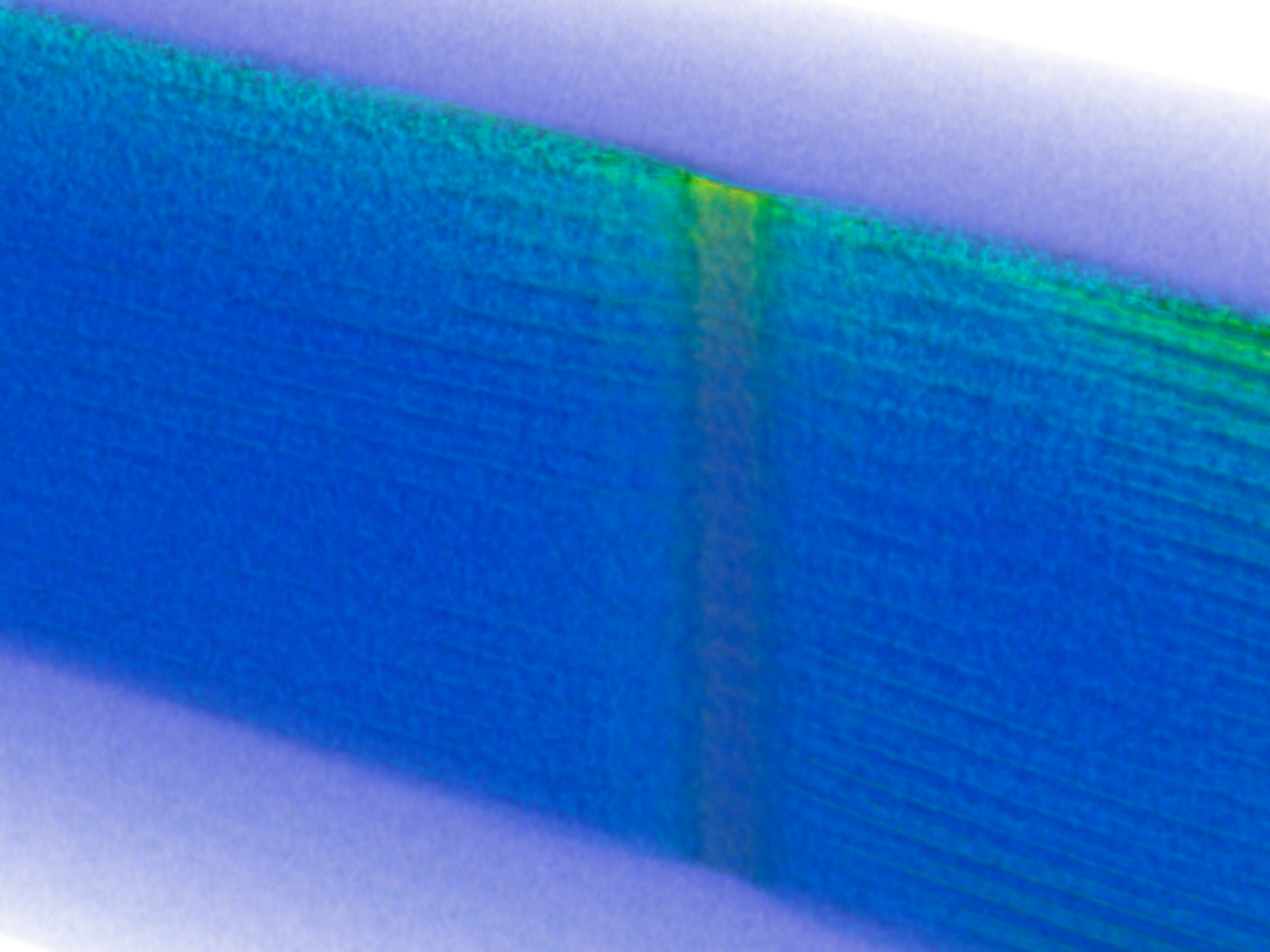
z

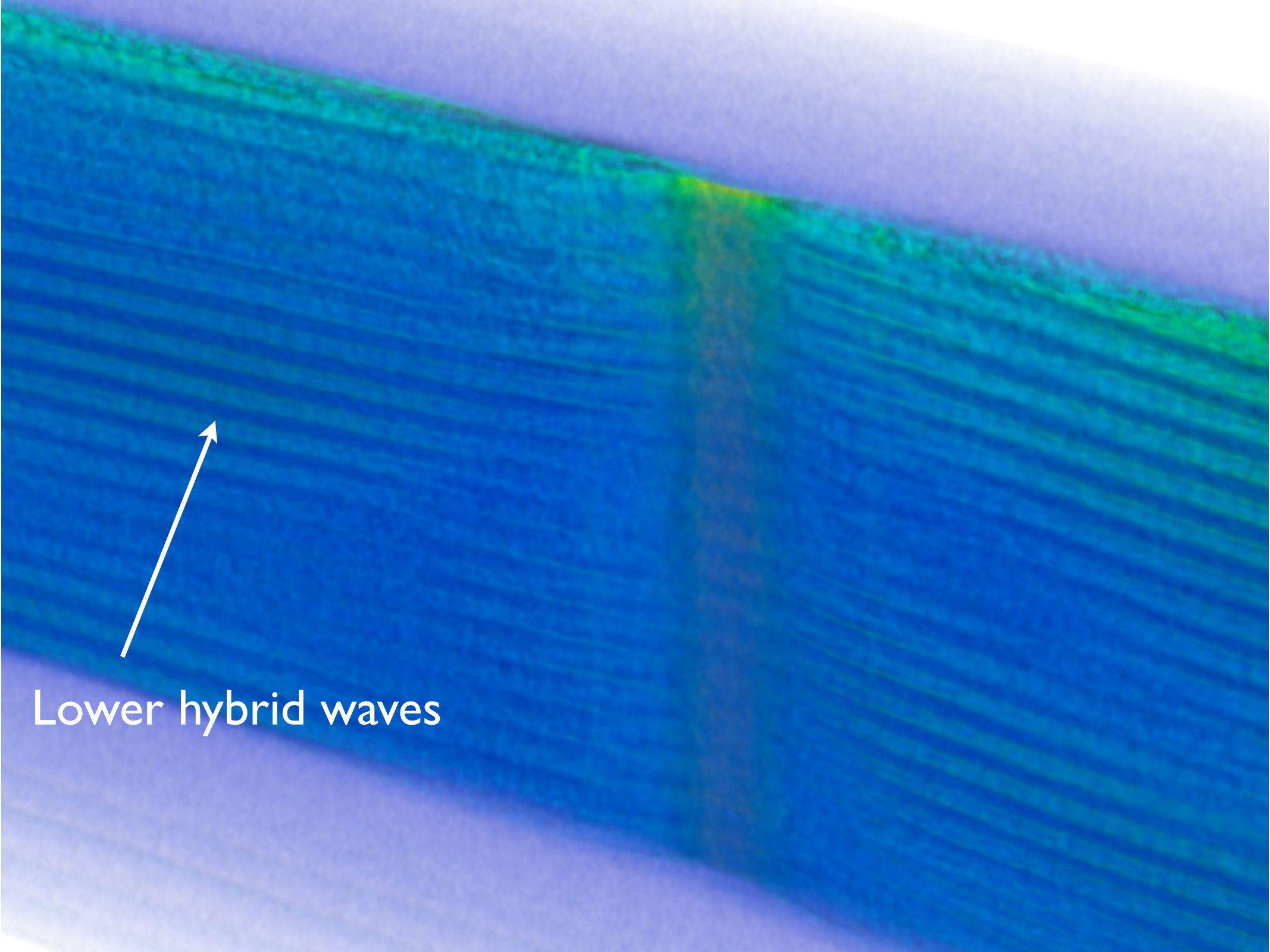
Initial Current sheet YZ plane



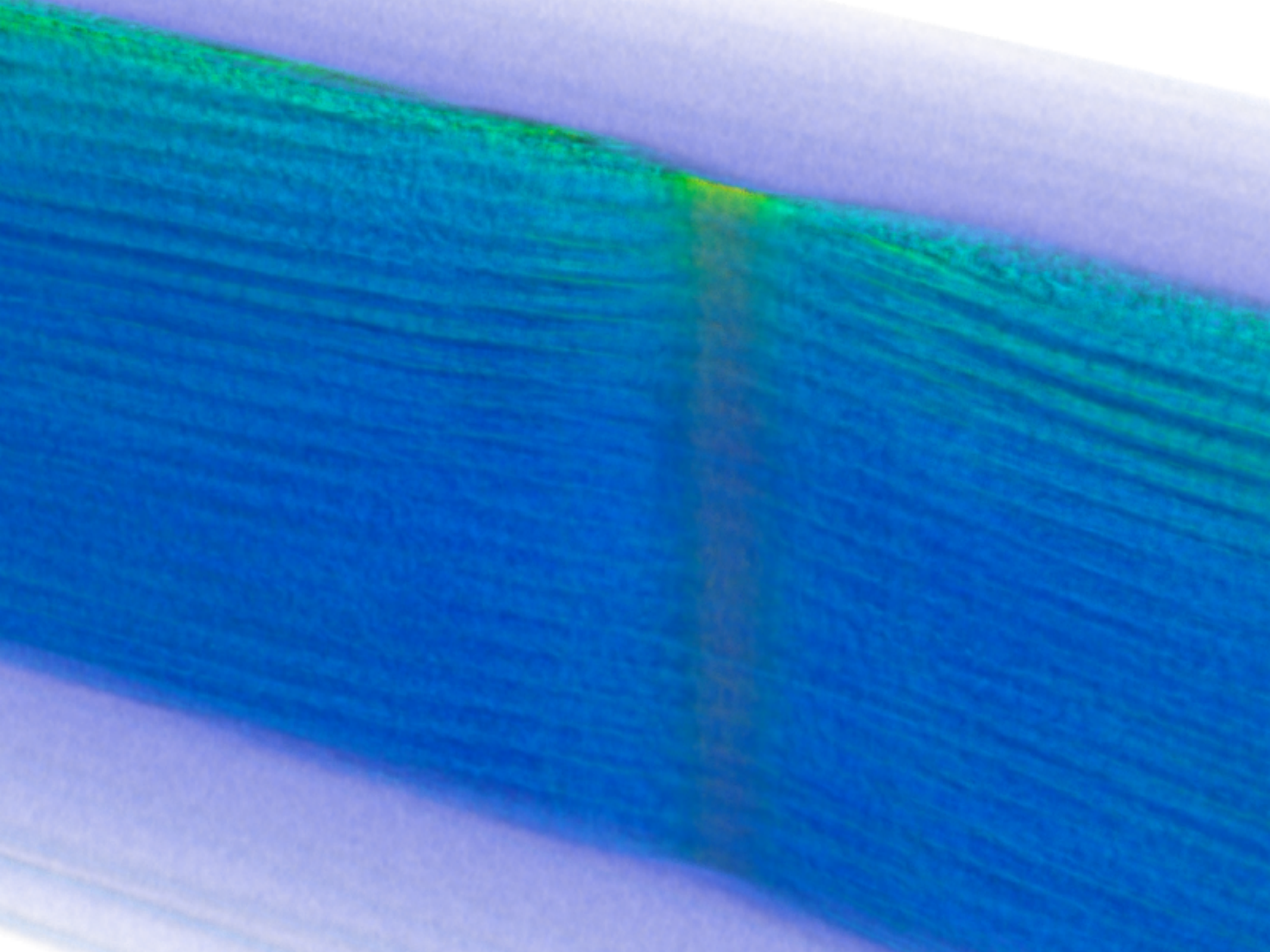
X-line perturbation

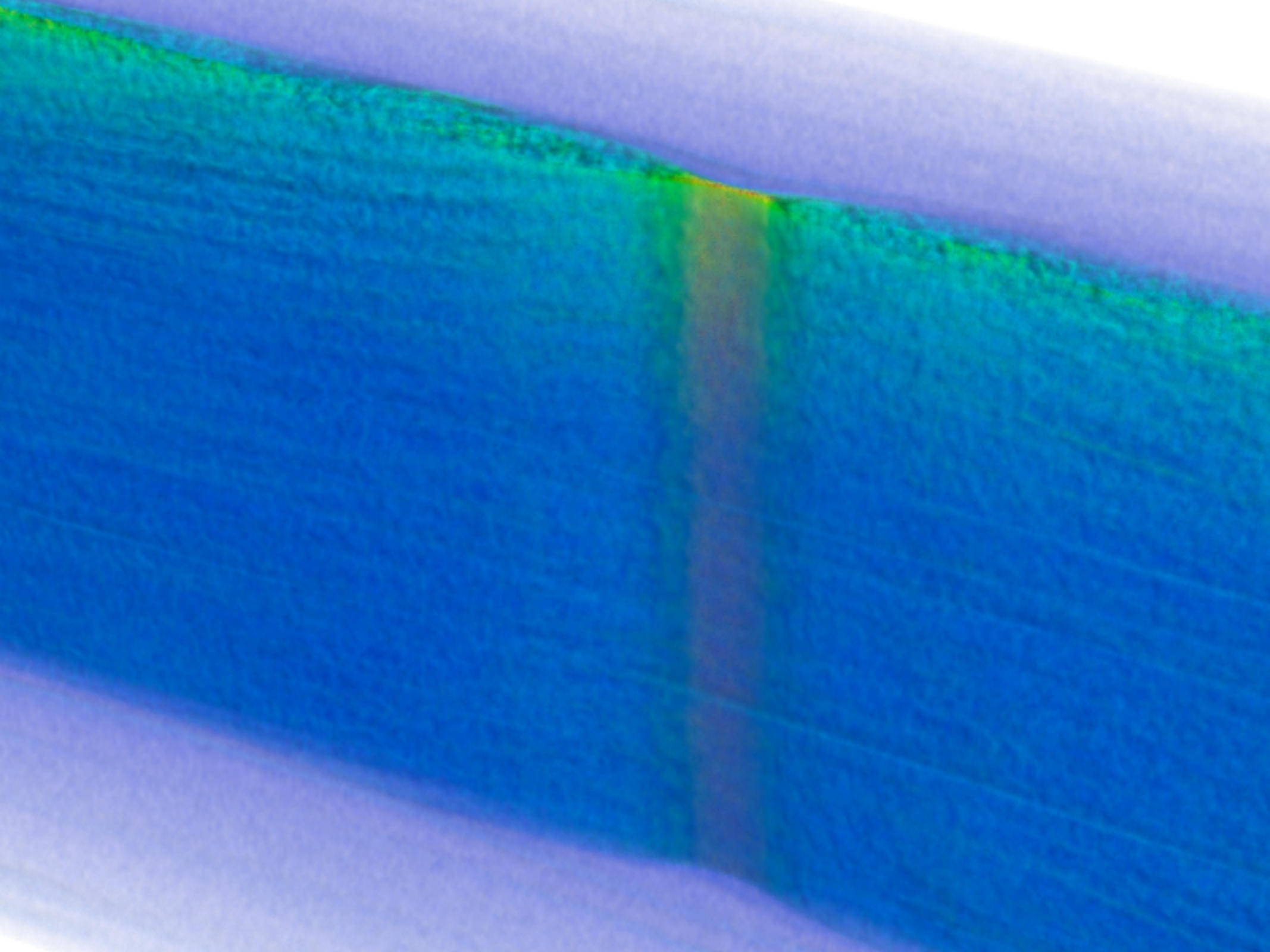


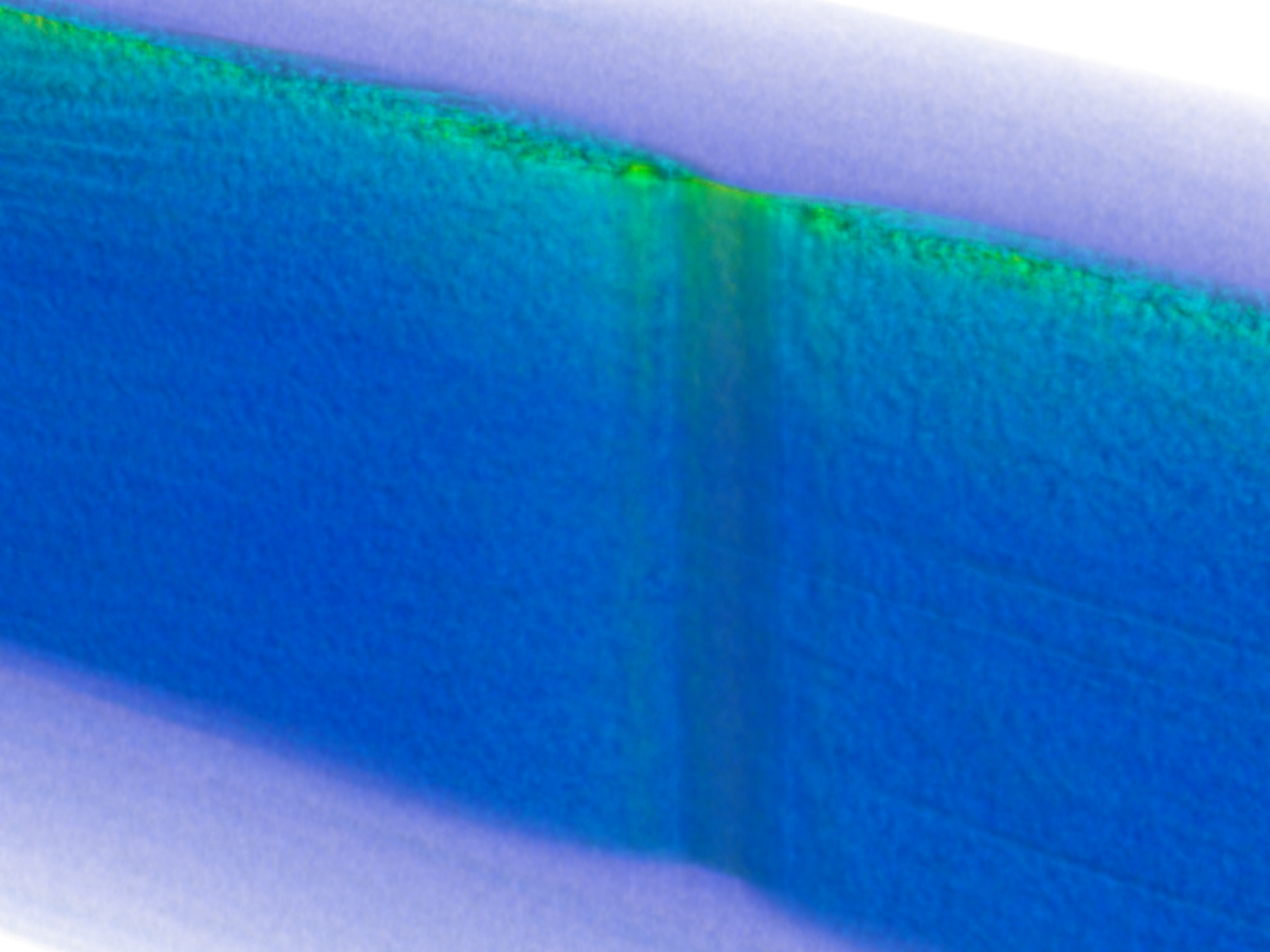


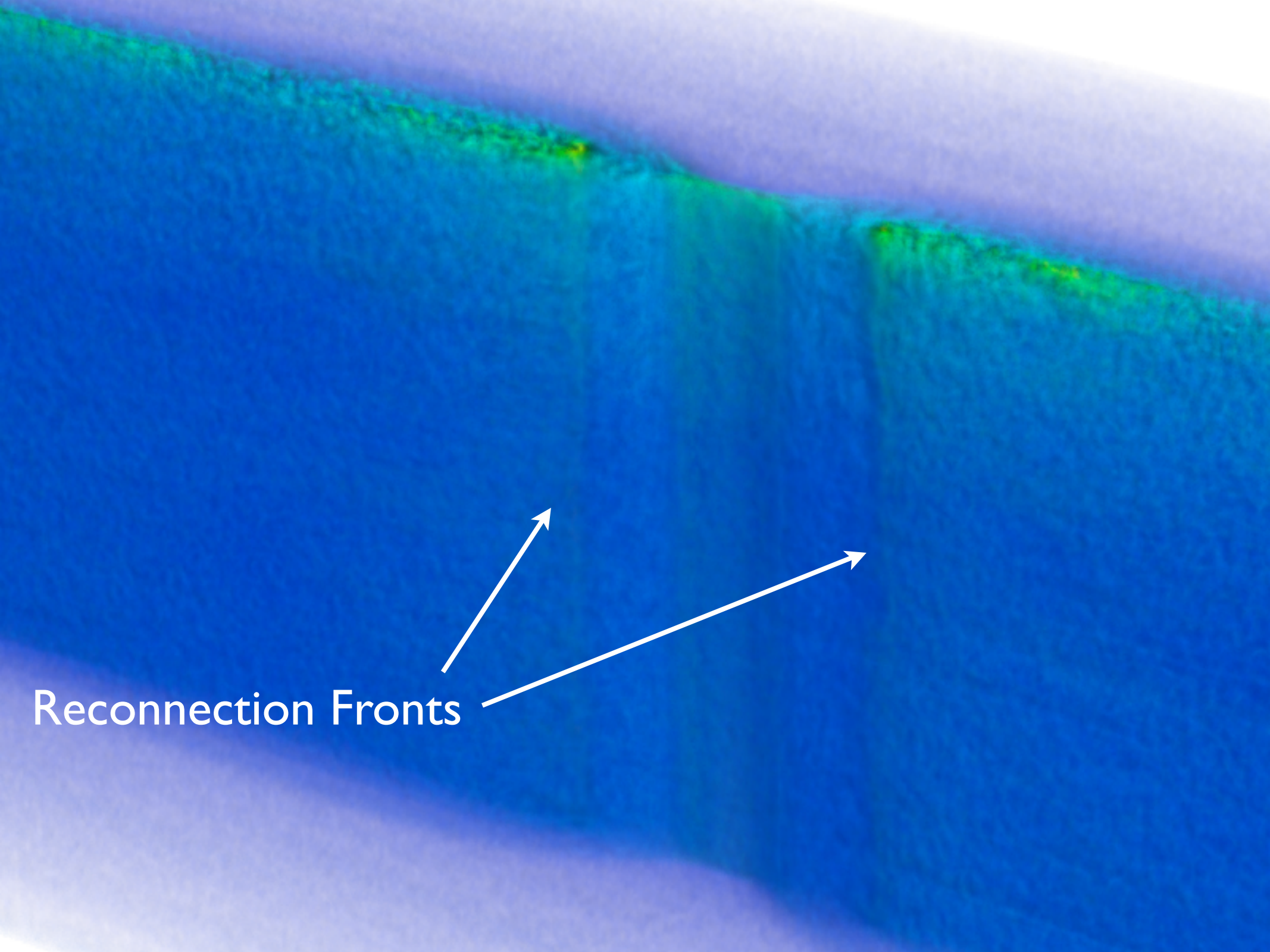


Lower hybrid waves



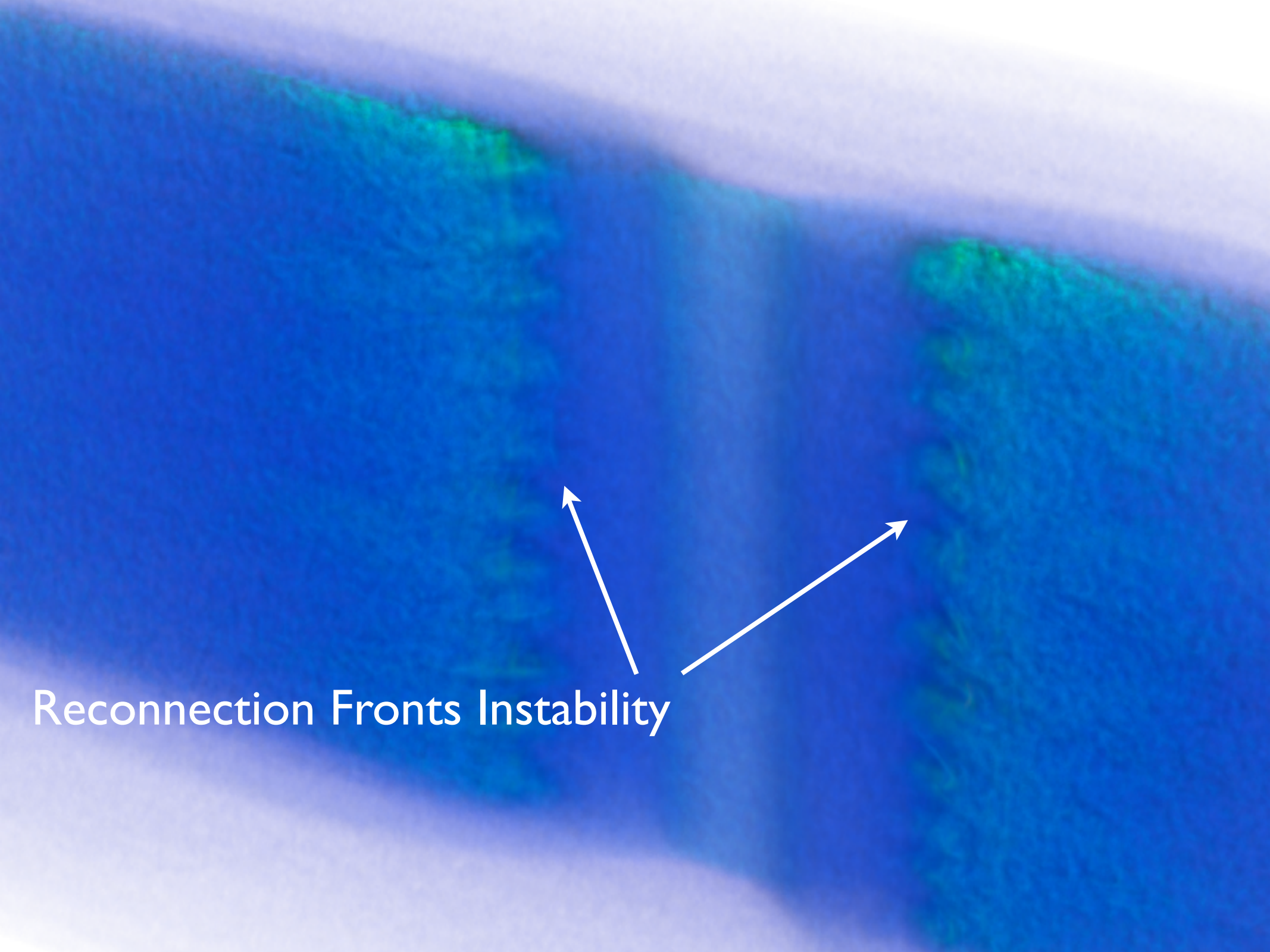




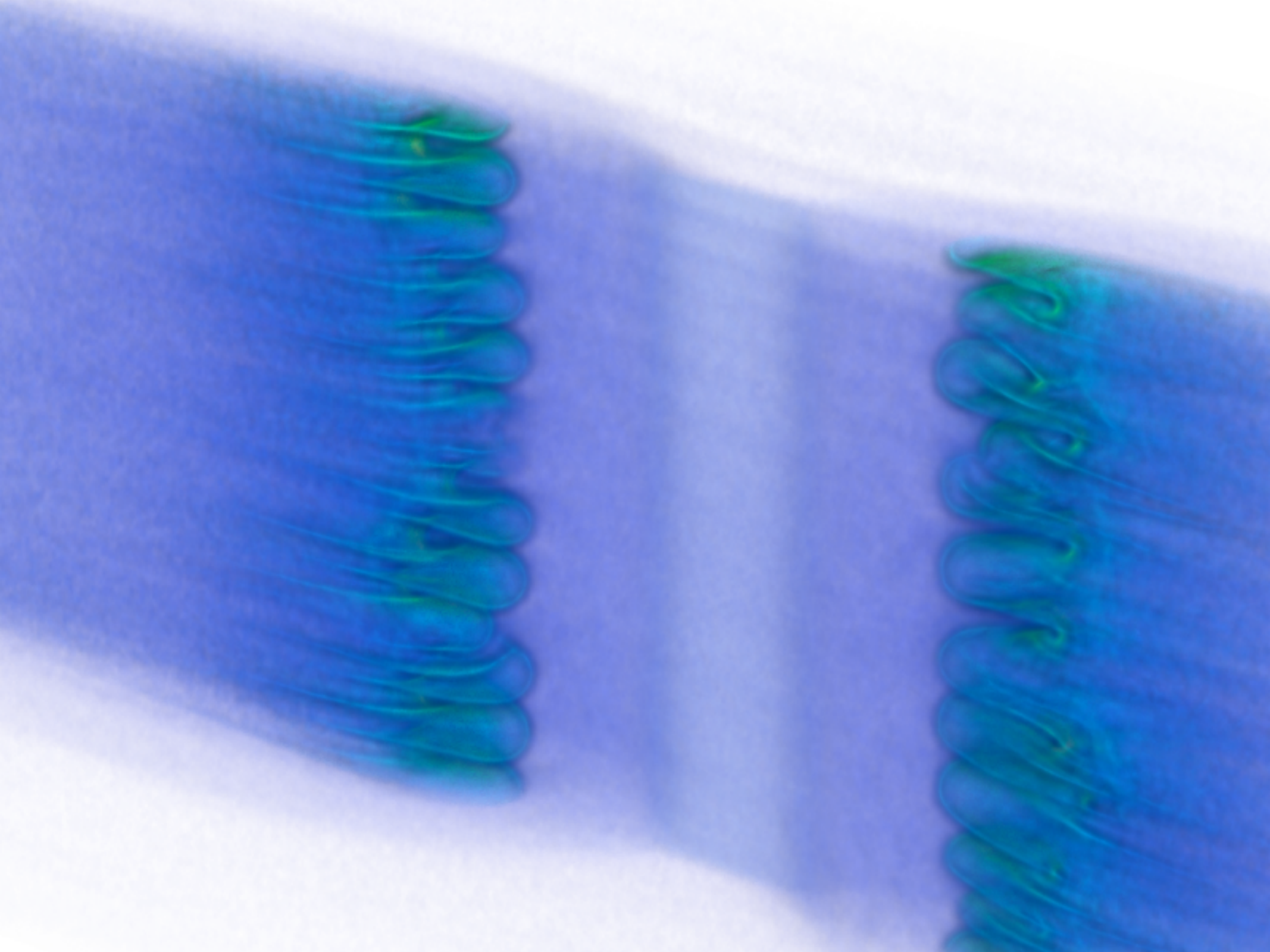


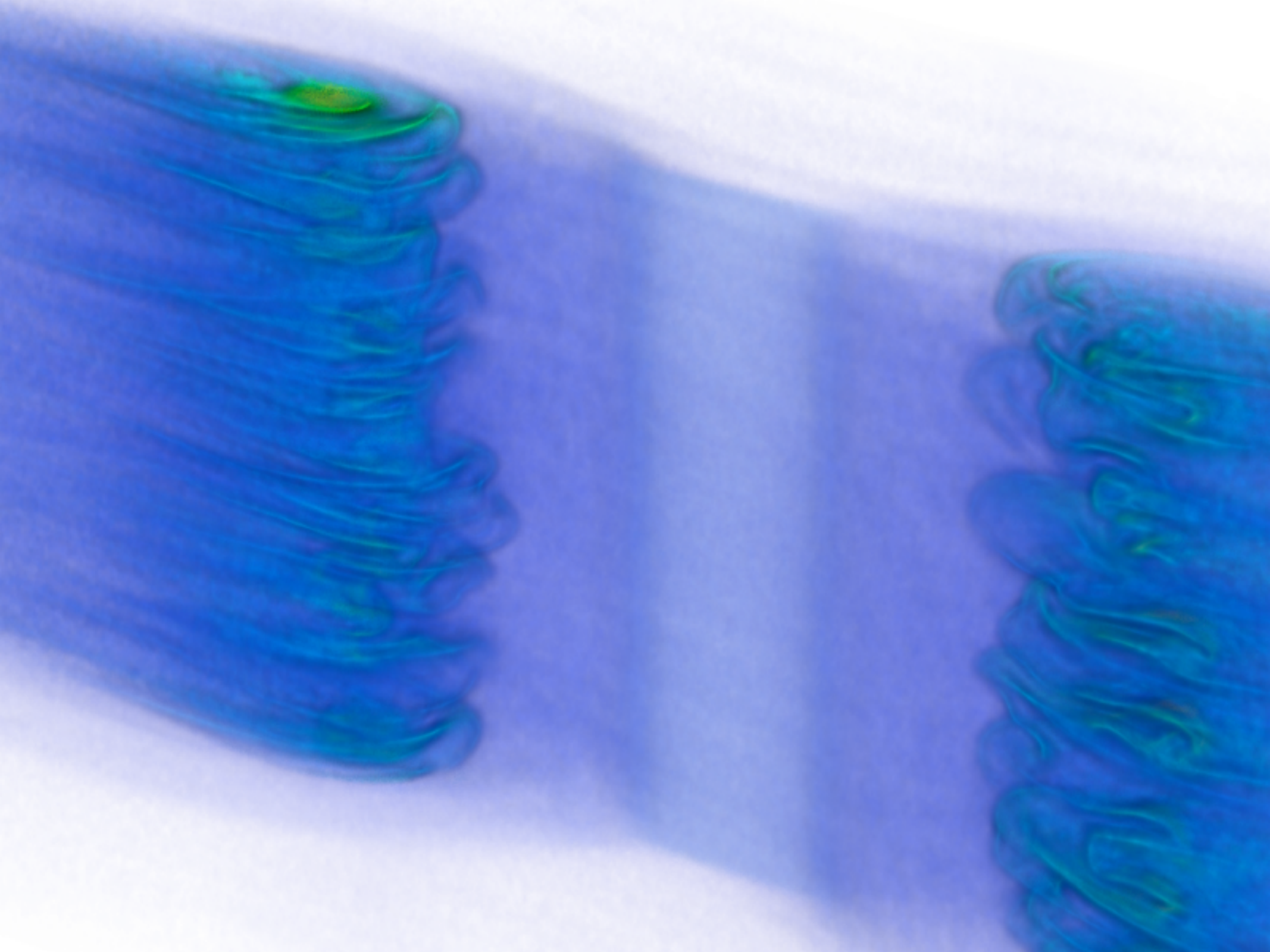
Reconnection Fronts

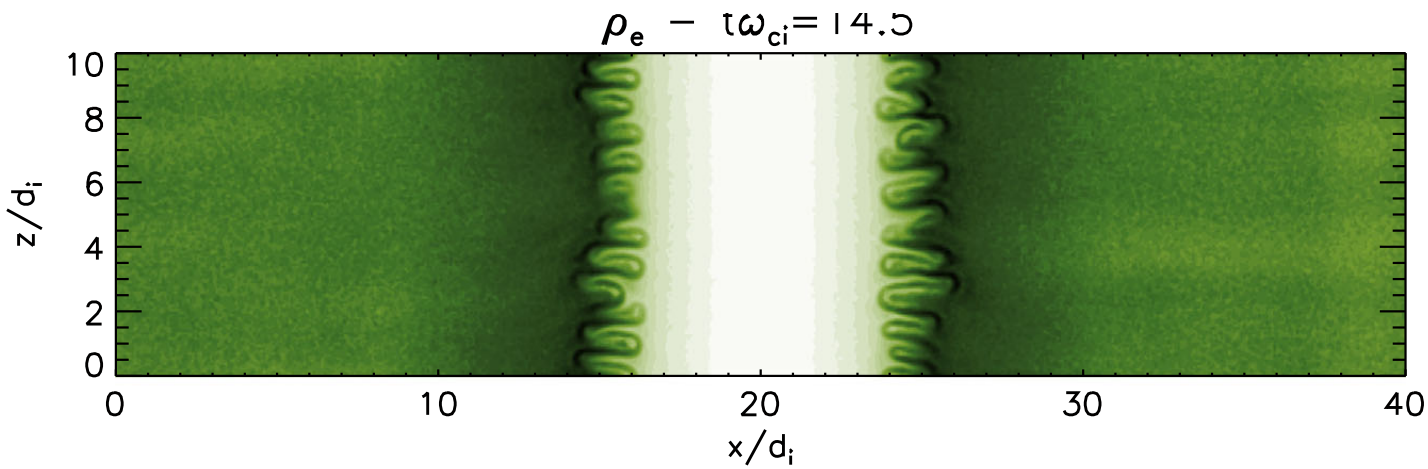




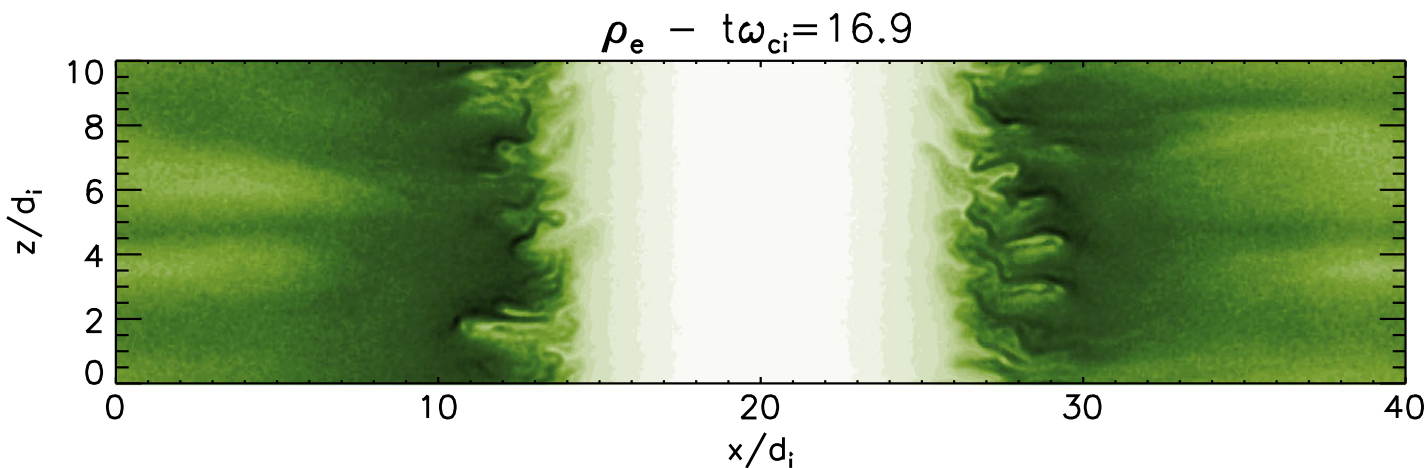
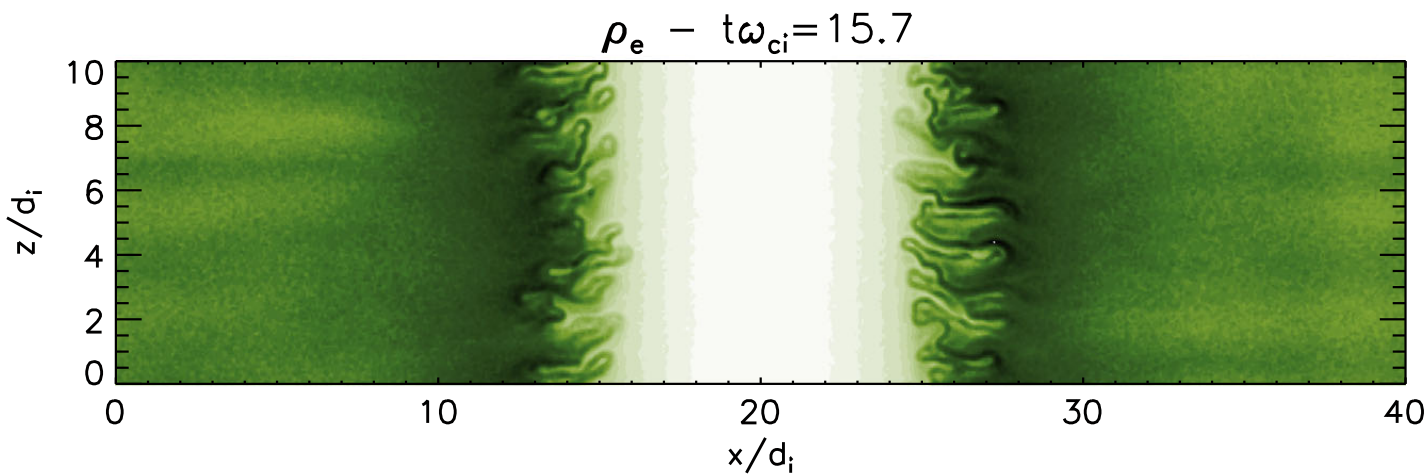
Reconnection Fronts Instability





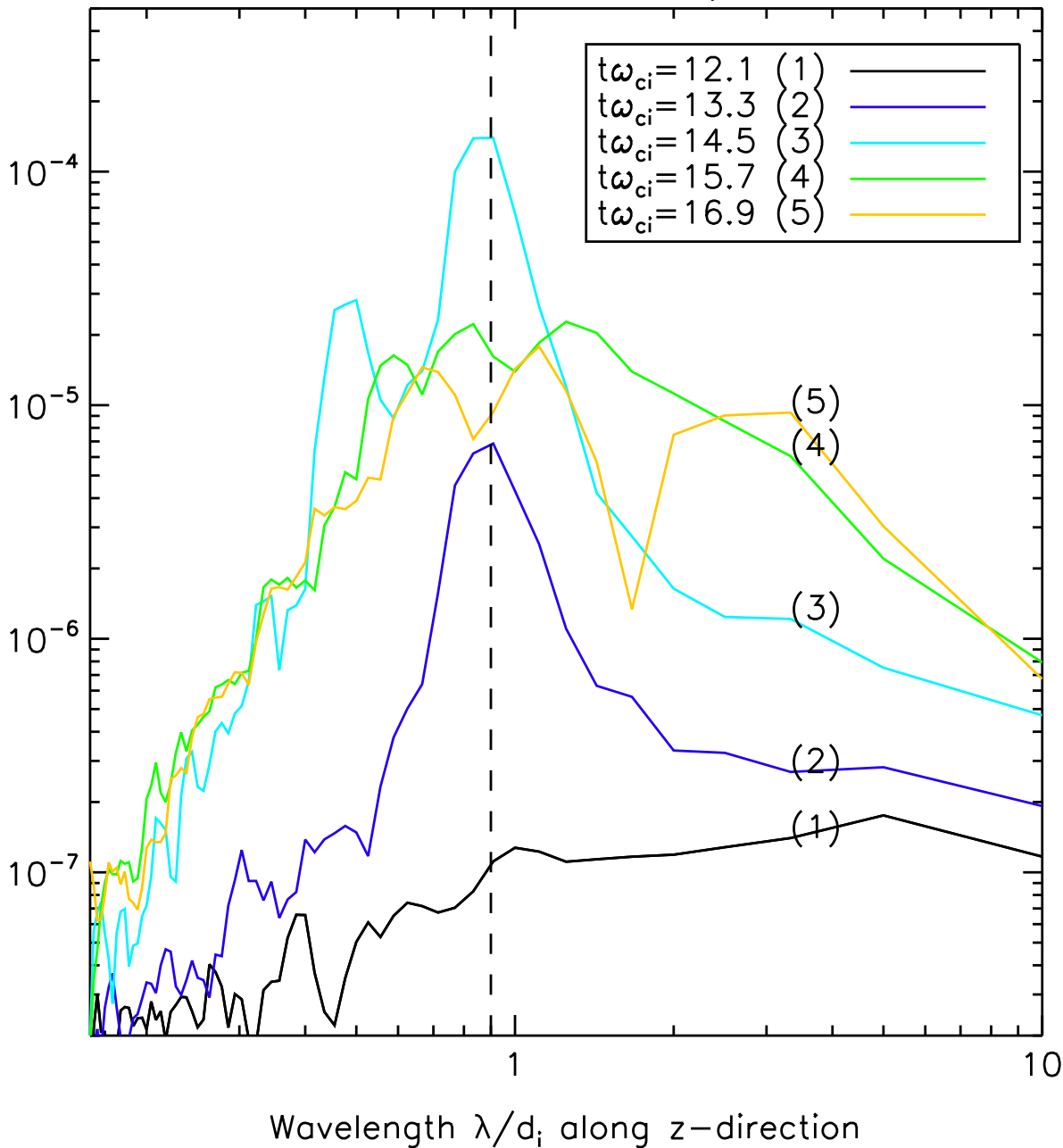


Iso-contours of the electron density in the XZ plane cut located at half-box length $y = Ly/2$.



The instability develops at the location of the high density gradients and generates typical finger signatures of a (Rayleigh-Taylor-like) interchange instability. The instability wave vector (along Z) is perpendicular to both the local density gradient (along X) and the local magnetic field direction (along Y), as required for electrostatic drift instabilities. The instability eventually saturates reducing the density gradient.

Evolution of electron velocity V_x spectrum



Spectrum of the electron velocity $V_{x,e}$ as a function of the wavelength computed along Z direction at the location of the unstable front of high density gradient. The spectrum is initially flat. Then the instability peak appears (blue line 2) and grows (light blue line 3) at the most unstable wavelength $|d_i|$. The instability eventually saturates (line 4), generating disturbances at larger wavelengths (line 5).

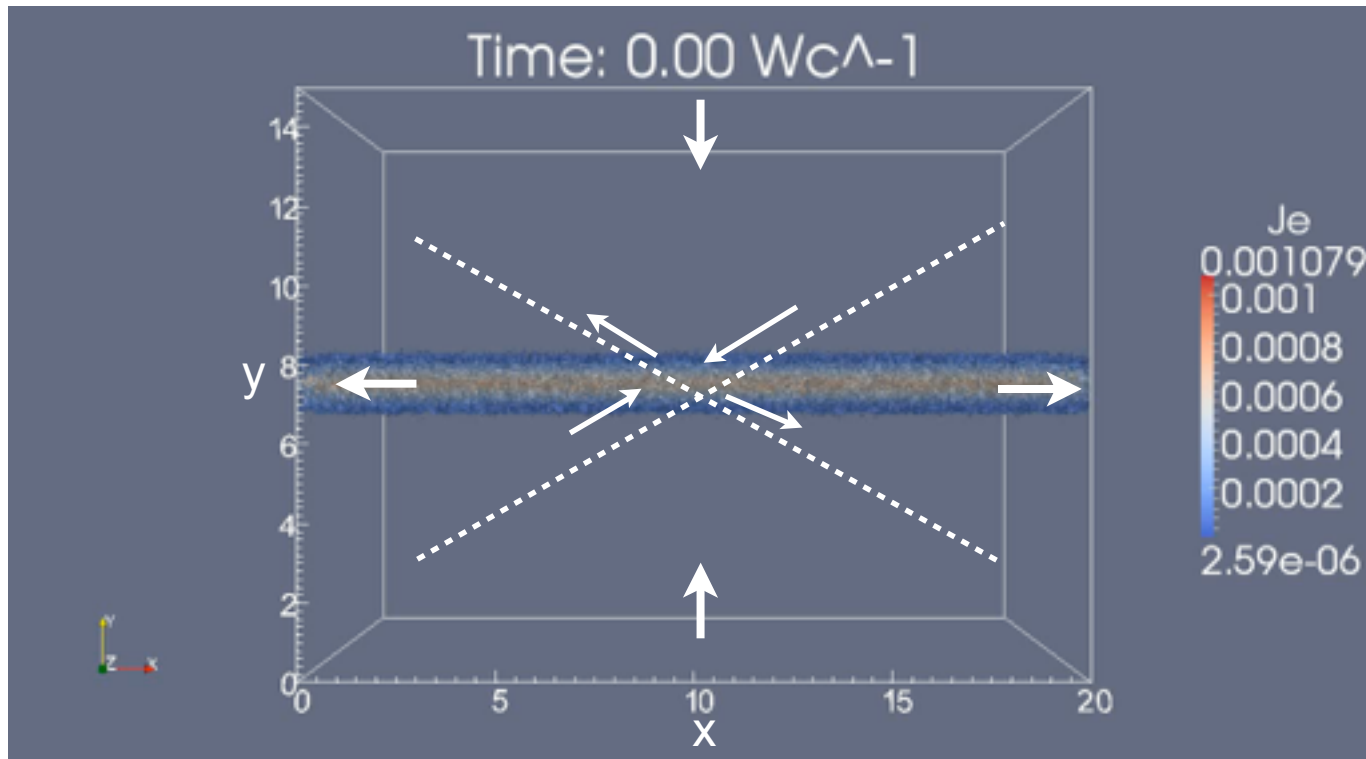
Given the wavelength value $|d_i|$, the instability is in its short wavelength regime, called the **kinetic interchange instability**.

The small wavelength enables to decouple electron and ion velocities, thus generating an associated Hall electric field that can enhance anomalous transport along the reconnection front.

2- Harris Equilibrium with a Guide Field

- Focus on instabilities affecting magnetic reconnection separatrices and structure of density cavities.
- Motivation: possible signatures of proximity to magnetic reconnection sites.
- Reference papers:
 - Markidis, Stefano, Giovanni Lapenta, Andrey Divin, M. Goldman, D. Newman, and Laila Andersson. "Three dimensional density cavities in guide field collisionless magnetic reconnection." *Physics of Plasmas* 19 (2012): 032119.
 - Divin, Andrey, Giovanni Lapenta, Stefano Markidis, D. L. Newman, and M.V. Goldman. "Numerical simulations of separatrix instabilities in collisionless magnetic reconnection." *Physics of Plasmas* 19 (2012): 042110.

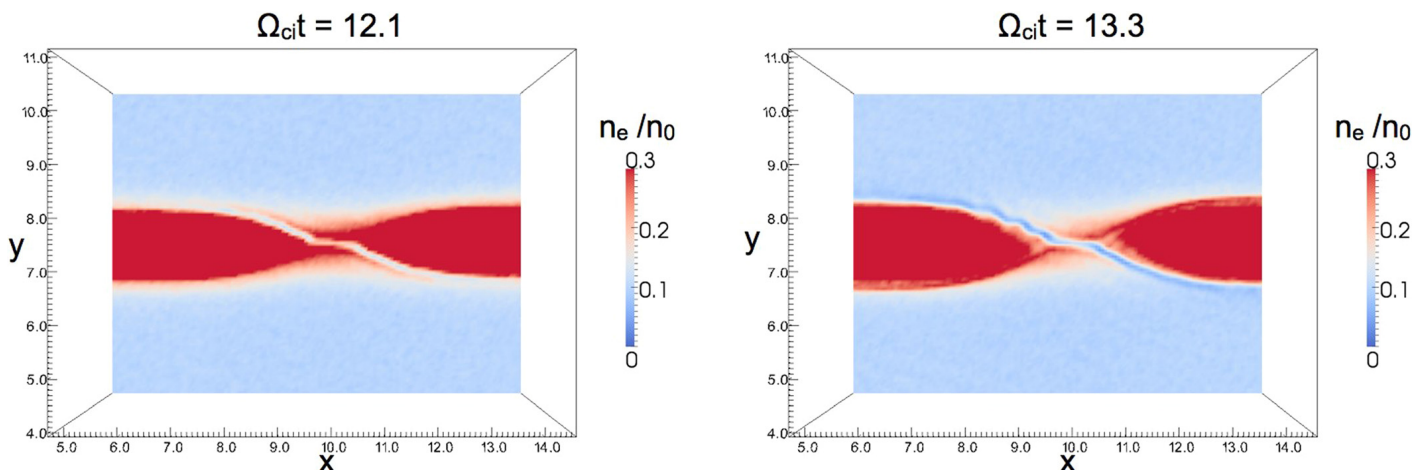
Separatrices and Cavities



The surfaces between the new magnetic regions, dividing the inflow and outflow plasmas are called separatrices.

One of the distinctive features of collisionless magnetic reconnection is the formation of localized low density regions along the separatrices called **cavities**.

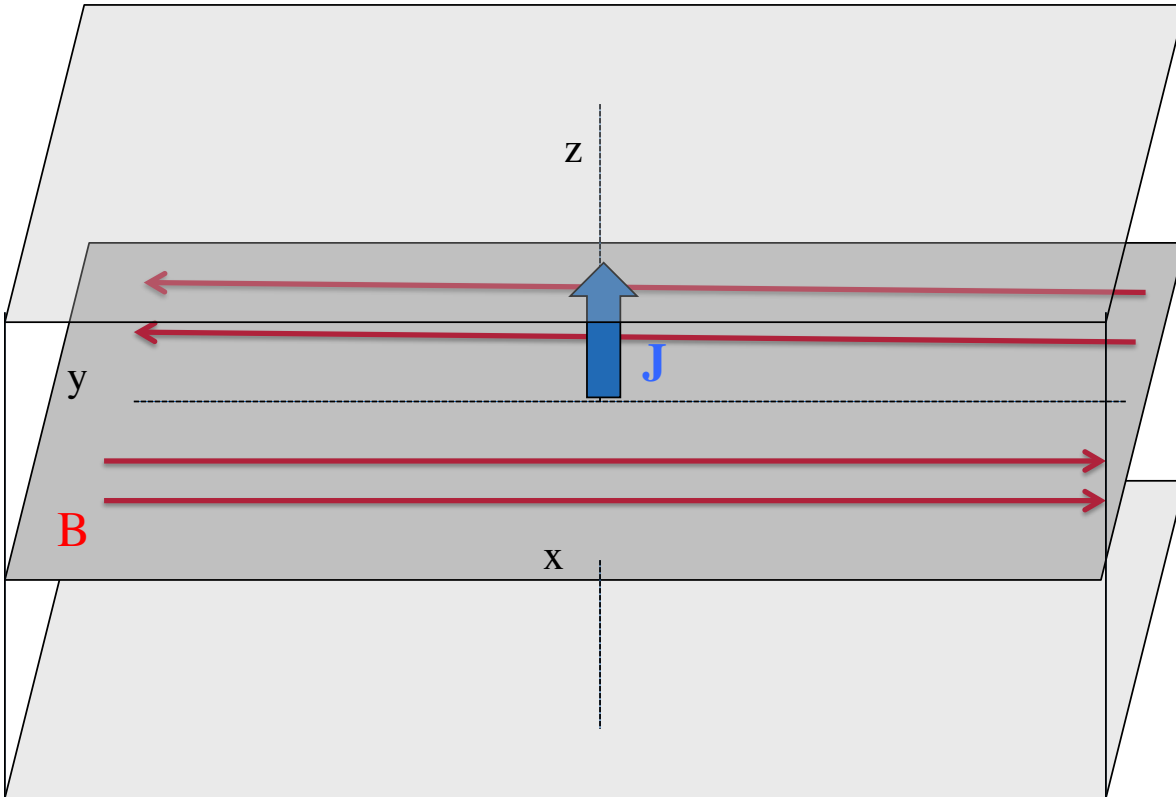
In presence of guide field, separatrices display anti-symmetric features with respect to the X line: the cavities develop only along two separatrices. In addition, strong electron beams move toward the X line along the cavities separatrices



Simulation Set-Up

$$B_x(y) = B_0 \tanh\left(\frac{y - L_y/2}{\lambda}\right)$$

$$n(y) = n_0 \cosh^{-2}\left(\frac{y - L_y/2}{\lambda}\right) + n_b$$



A uniform magnetic field (guide field) $B_g = B_0$ in the z direction is added.

$$L_x = 20 d_i$$

$$L_y = 15 d_i$$

$$L_z = 10 d_i$$

$$n_{xc} \times n_{yc} \times n_{zc} = 256 \times 192 \times 128$$

Periodic BC in x and z

Perfect conductor BC in y

$$n_b = 0.1 n_0$$

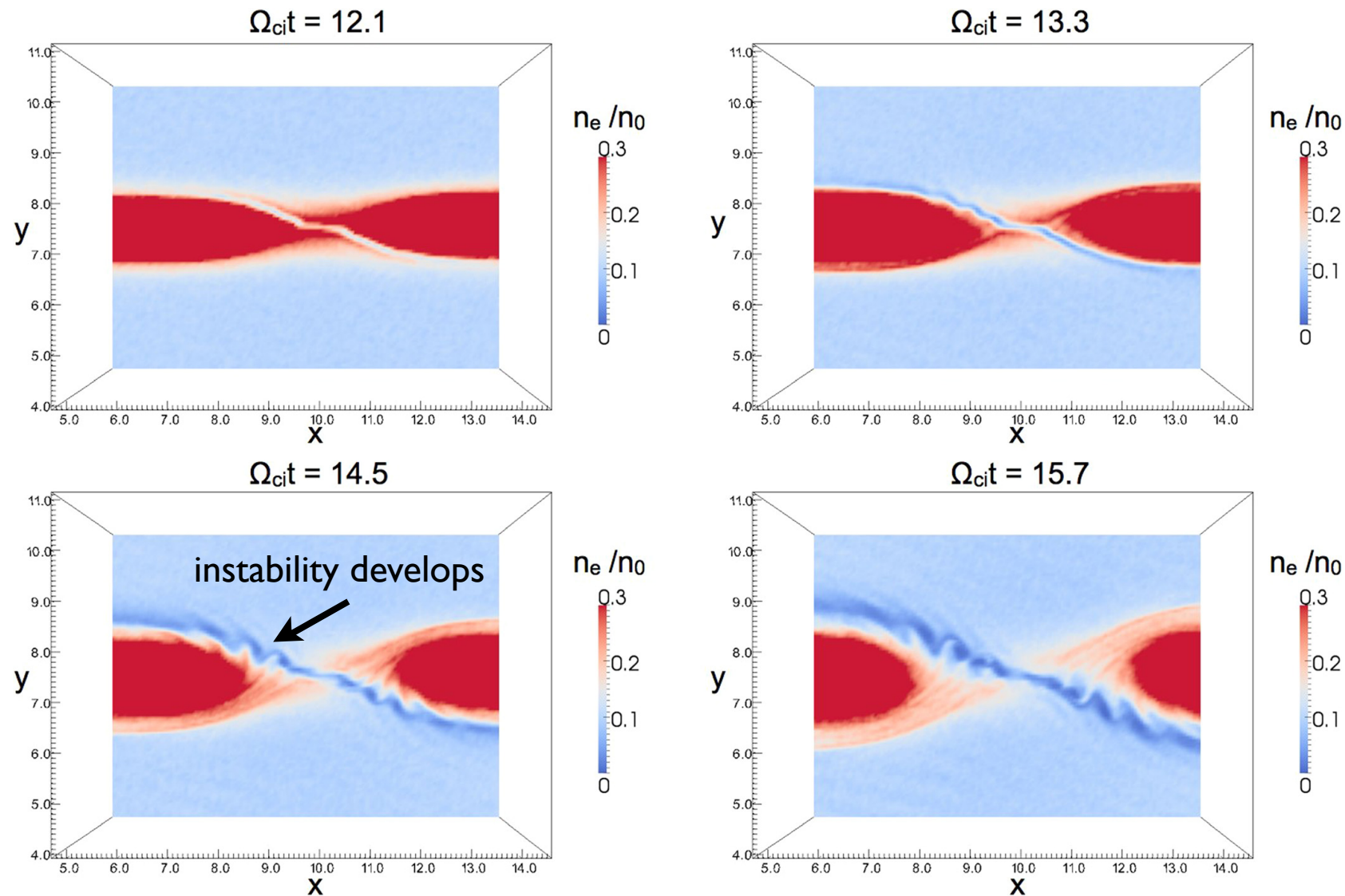
$$\Delta t = 0.125 \omega_{pi}^{-1}$$

$$m_i/m_e = 256$$

$$n_p = 3 \times 10^9$$

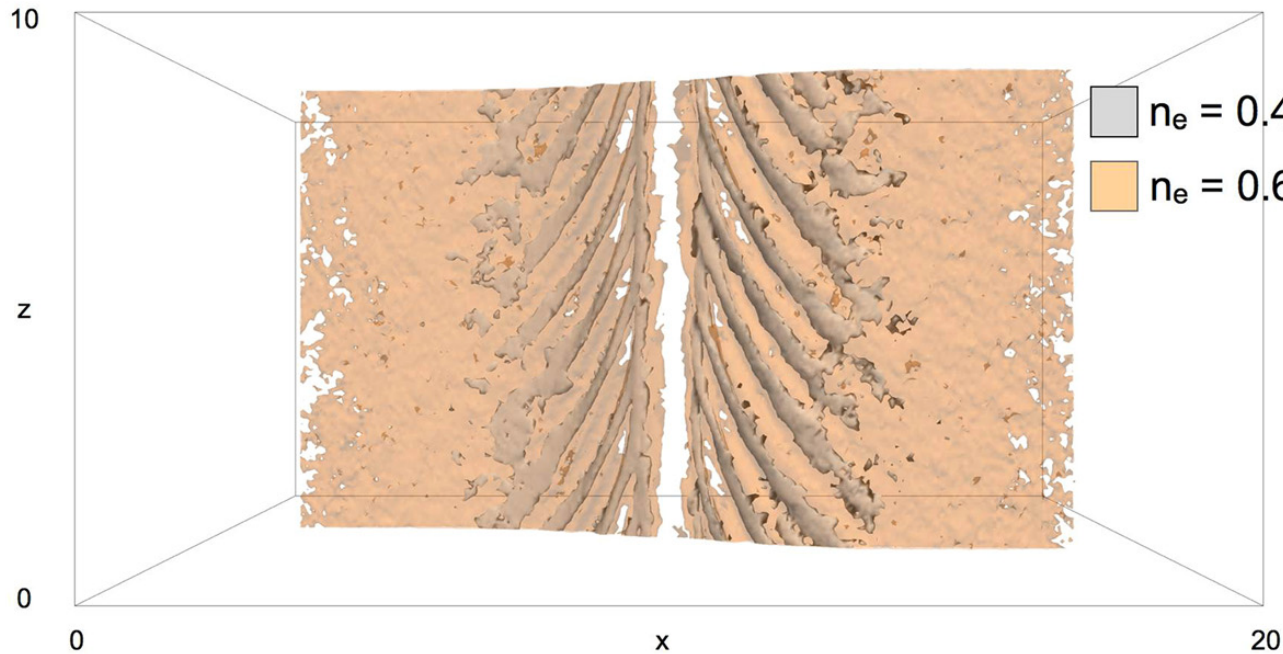
Initial Perturbation along the dashed line.

Evolution of Density Cavities



The plot shows the formation of the density cavity layers (blue regions), and the successive development of density ripples, reminiscent of Kelvin-Helmholtz vortices, along the cavities.

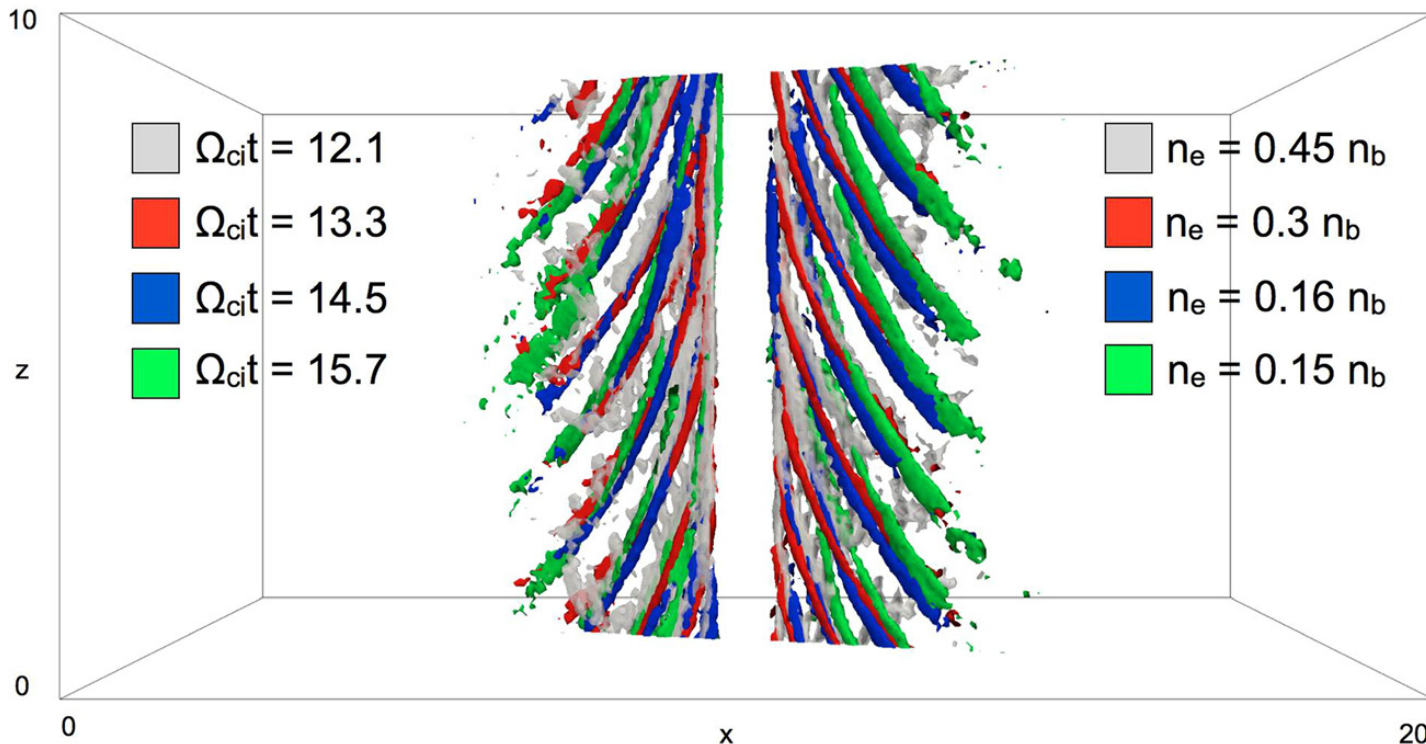
a)



$n_e = 0.4 n_b$ = sub-cavities or low density ribs
 $n_e = 0.65 n_b$ = cavities

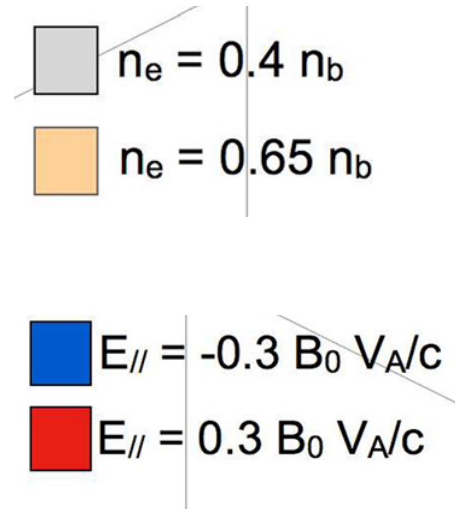
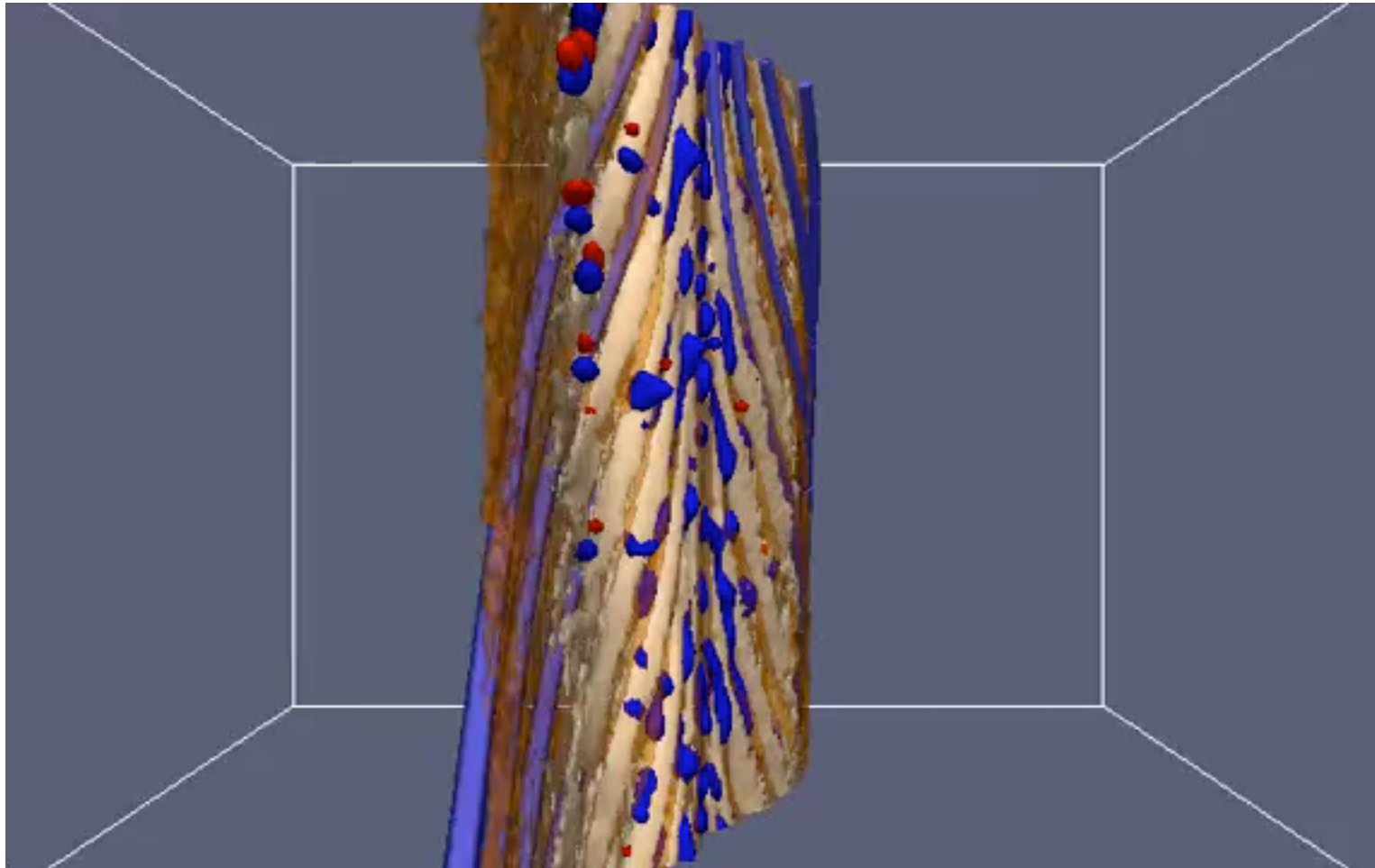
The isosurface $n_e = 0.65 n_b$ shows the cavity layer, the isosurface $n_e = 0.4 n_b$ reveals that regions with further lower density are embedded in the cavities.

b)



The location of the low density ribs is approximately fixed in time, and their density progressively decreases.

Electric field bipolar structures localized along separatrixes



The bipolar parallel electric field structures develop along cavities as effect of streaming instabilities.

2D PIC simulation studies suggest that this instability is an electron MHD Kelvin-Helmholtz of the electron channel.

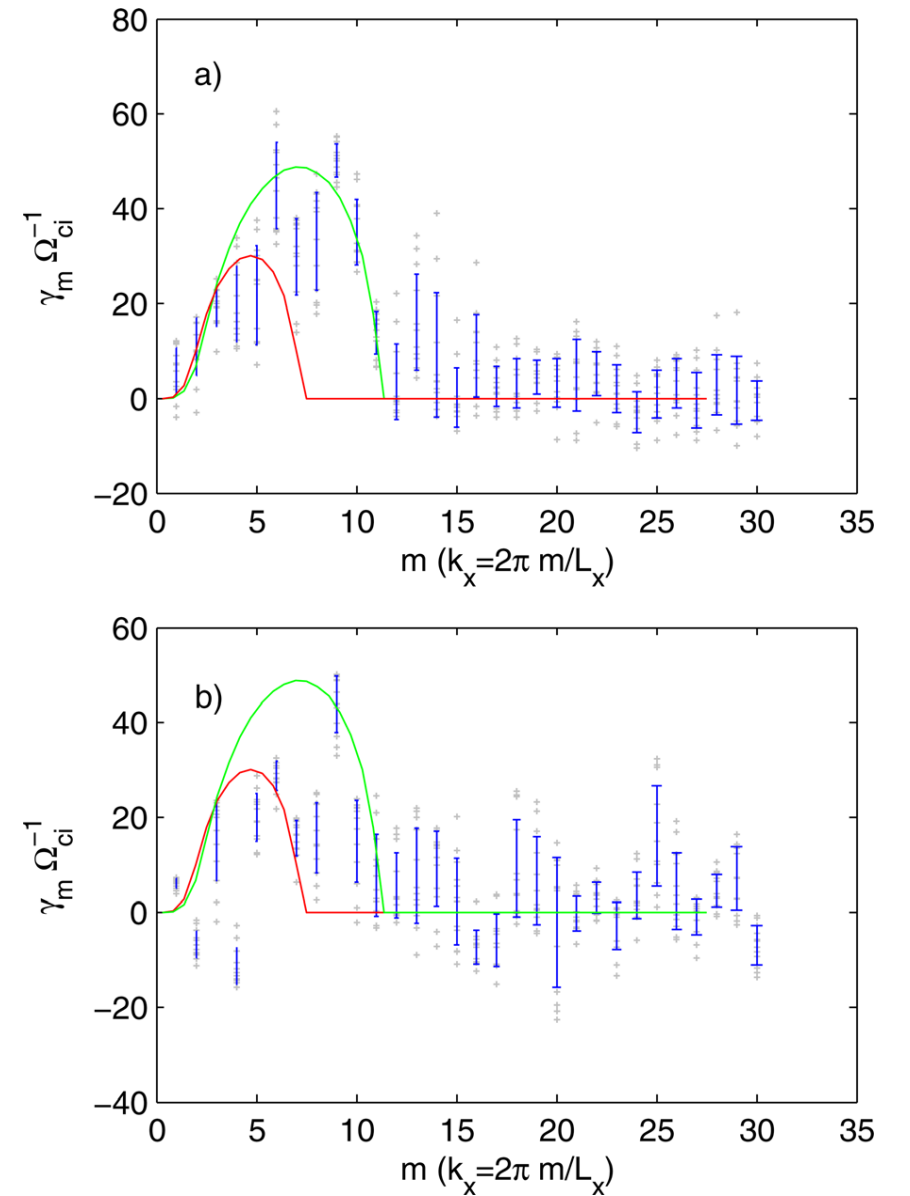


FIG. 13. Growth rate estimates for the modes $1 \leq m \leq 30$ of $v_{e\perp 1}$ electron velocity component (a) and B_y component (b) in the $(\vec{e}_{\perp 1}, \vec{e}_{\perp 2})$ plane simulation. A total of 12 profiles are taken, distributed evenly in the interval $0.8 \leq y/d_i \leq 0.9$ that covers the entire $v_{e\perp 2}$ flow reversal. Red line: growth rate estimate (Eq. (6)), for a set of parameters: $n_{e0} = 0.02$, $V_{x0} = 4.0V_A$, $\varepsilon = 0.025 d_i$ (thin red line) and $n_{e0} = 0.02$, $V_{x0} = 4.0V_A$, $\varepsilon = 0.016 d_i$ (bold green line).

The fine structure of the cavities has been observed in the magnetotail.

Observation of multiple sub-cavities adjacent to single separatrix

Rongsheng Wang,¹ Aimin Du,¹ Rumi Nakamura,² Quanming Lu,³ Yuri V. Khotyaintsev,⁴ Martin Volwerk,² Tielong Zhang,² E. A. Kronberg,⁵ P. W. Daly,⁵ and Andrew N. Fazakerley⁶

Received 13 April 2013; revised 3 May 2013; accepted 4 May 2013.

[1] We investigate a direct south-north crossing of a reconnection ion diffusion region in the magnetotail. During this crossing, multiple electron density dips with a further density decrease within the cavity, called sub-cavities, adjacent to the northern separatrix are observed. The correlation between electron density sub-cavities and strong electric field fluctuations is obvious. Within one of the sub-cavities, a series of very strong oscillating perpendicular electric field and patchy parallel electric field are observed. The parallel electric field is nearly unipolar and directs away from X line. In the same region, inflow electrons with energy up to 100 keV are injected into the X line. Based on the observations, we conclude that the high-energy inflowing electrons are accelerated by the patchy parallel electric field. Namely, electrons have been effectively accelerated while they are flowing into the X line along the separatrix. The observations indicate that the

Khotyaintsev et al., 2006; *Retinò et al.*, 2006; *Lu et al.*, 2010; *Zhou et al.*, 2011; *Wang et al.*, 2012] and might play a key role in accelerating electrons [*Drake et al.*, 2005; *Divin et al.*, 2012; *Wang et al.*, 2012]. Within the density cavity, streaming of low energy electrons as a part of Hall current system is detected frequently [*Nagai et al.*, 2001; *Nakamura et al.*, 2008; *Wang et al.*, 2010]. Recently, *Wang et al* [2012] found that the energy of the streaming can be as high as 20 keV. The observations indicate that electrons may have been pre-accelerated in the separatrices. However, the fine structure and how electrons are accelerated in the cavity are still open questions.

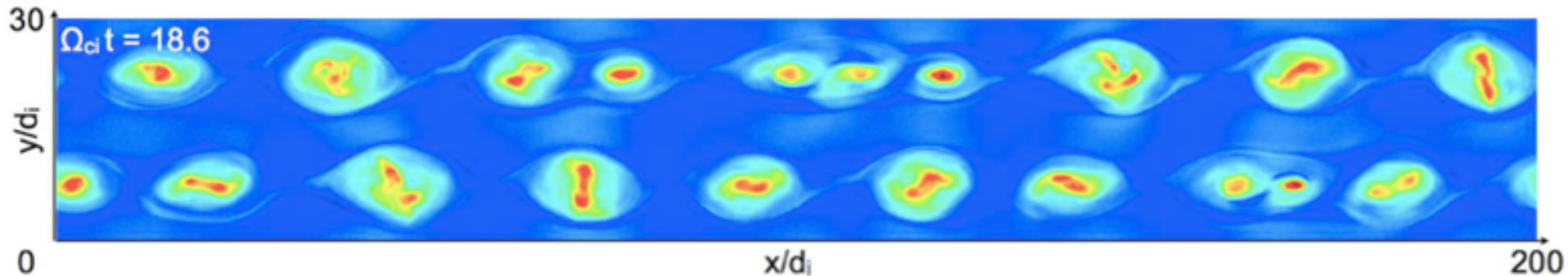
[3] In this letter, we present a reconnection event observed by Cluster [*Escoubet et al.*, 1997] in the magnetotail and analyze the density cavity in detail during one simple crossing tailward of the X line. Except for a series of patchy parallel electric field observed in the cavity, the prominent signature

3 - Plasmoid Chain Dynamics

- Three dimensional evolution of plasmoid chain dynamics.
- References papers:
 - Markidis, Stefano, Pierre Henri, Giovanni Lapenta, Andrey Divin, Martin Goldman, David Newman, and Erwin Laure. "Kinetic Simulations of Plasmoid Chain Dynamics." *accepted for publication, Physics of plasmas* (2013).
 - Markidis, Stefano, Pierre Henri, Giovanni Lapenta, Andrey Divin, Martin V. Goldman, David Newman, and Stefan Eriksson. "Collisionless magnetic reconnection in a plasmoid chain." *Nonlinear Geophysics* (2012).
 - Newman, D. L., M.V. Goldman, G. Lapenta, and S. Markidis. "Magnetospheric Reconnection in Modified Current-Sheet Equilibria." *Bulletin of the American Physical Society* 57 (2012).

Plasmoid Chain

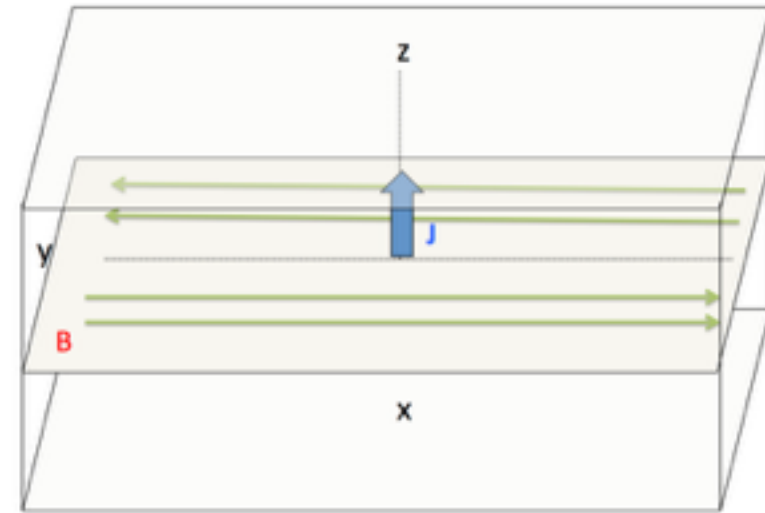
- Plasmoids are high density structures forming from the outflow plasma accelerated in magnetic reconnection. If magnetic reconnection occurs in multiple points, the outflow plasmas from adjacent reconnection sites form multiple plasmoids, organized as beads in a chain



- The effect of moderate guide field ($1/3 B_0$) is studied by comparing the results of two simulations with and without guide field in a configuration that mimics Earth magnetotail condition.

Simulation Set-up

- iPIC3D - **massively parallel implicit** Particle-in-Cell code is used for simulation on **12,288 cores**.
- Starting from Harris-like initial condition and **no perturbation**.
- **Two simulations** with and without a uniform magnetic field along z (**guide field**). The guide field is taken $1/3 B_0$.
- $L_x * L_y * L_z = 40c/\omega_{pi} * 15c/\omega_{pi} * 10c/\omega_{pi}$, $n_x * n_y * n_z = 512 * 384 * 128$, $8 * 10^9$ particles, $m_i/m_e = 256$, $T_i/T_e = 5$, $dt = 0.125 \omega_{pi}^{-1}$

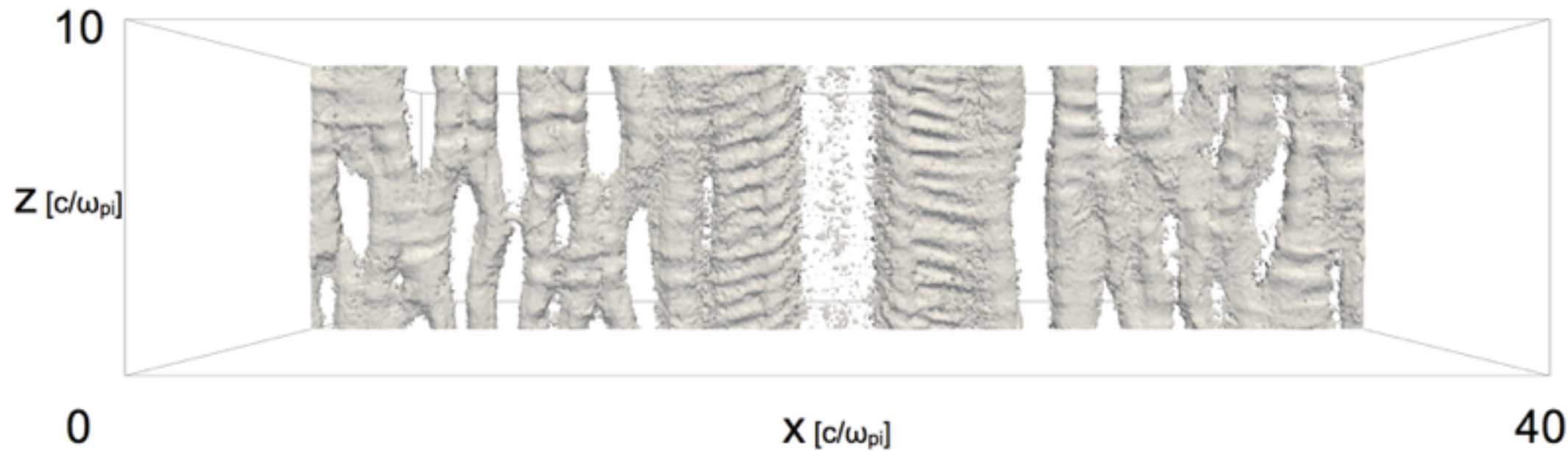


The initial configuration is not in equilibrium. The initial current J_z is 20% of the current necessary to support consistently the initial magnetic field. As result of this non-equilibrium, the plasma is initially accelerated toward the current sheet to establish a current consistent with the initial magnetic field configuration, accelerating the reconnection initiation.

Plasmoid chain dynamics in the
antiparallel case (no guide field)

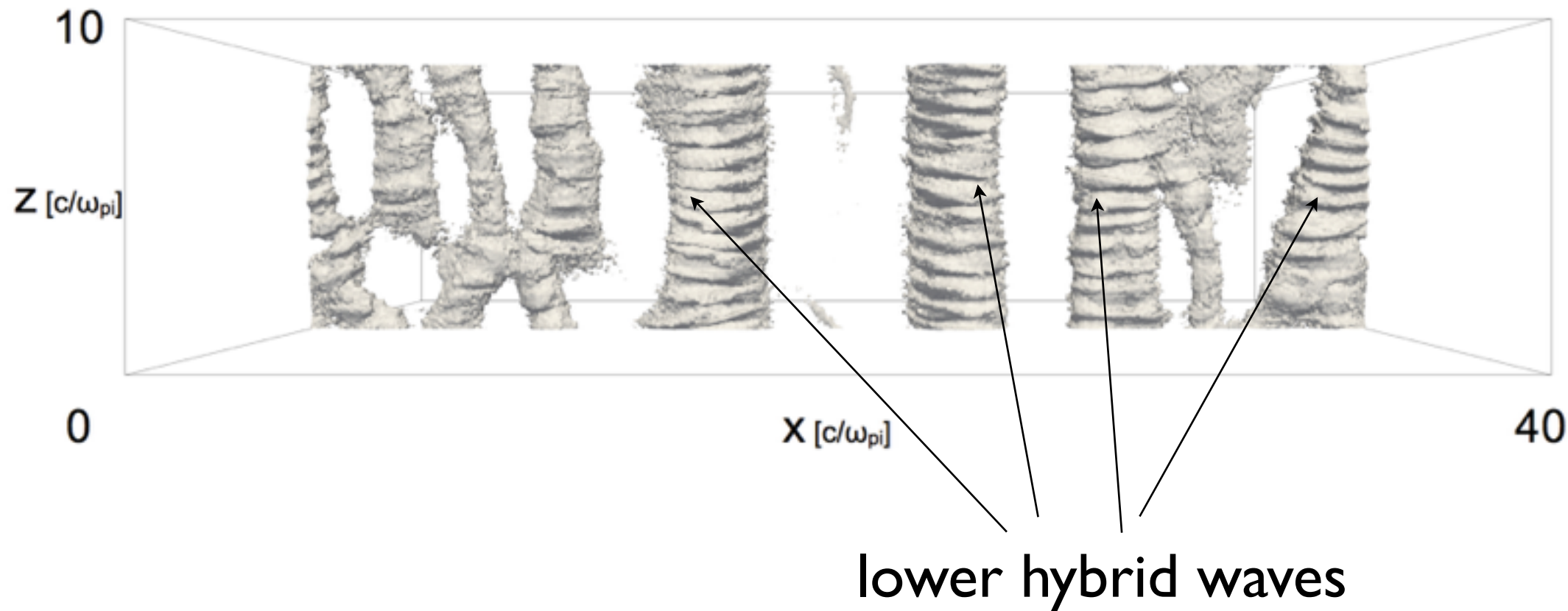
Electron density $n_e = 1.7 n_b$ (background density) $B_g = 0$

$$\Omega_{ci} t = 1.2$$



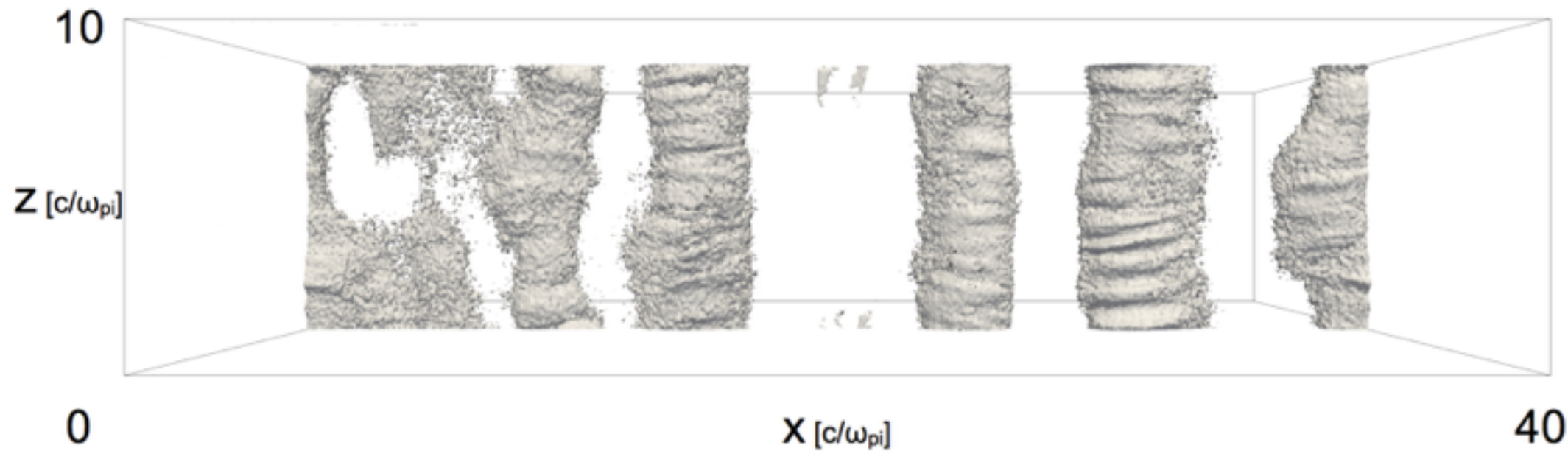
Electron density $n_e = 1.7 n_b$ (background density)

$$\Omega_{ci} t = 2.4$$



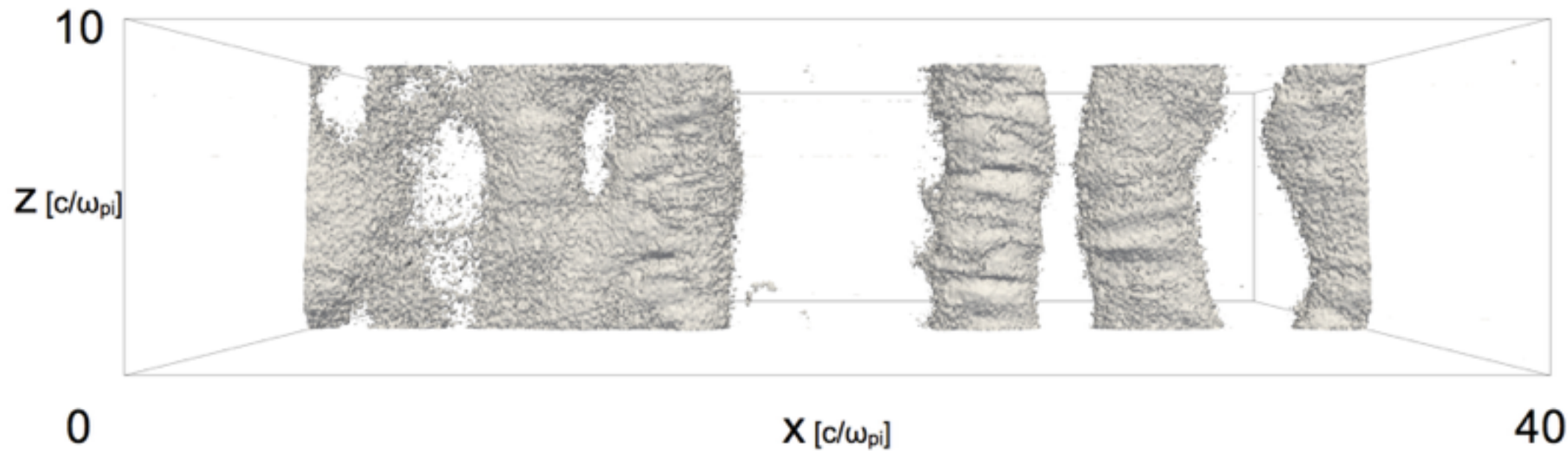
Electron density $n_e = 1.7 n_b$ (background density)

$$\Omega_{ci}t = 3.6$$



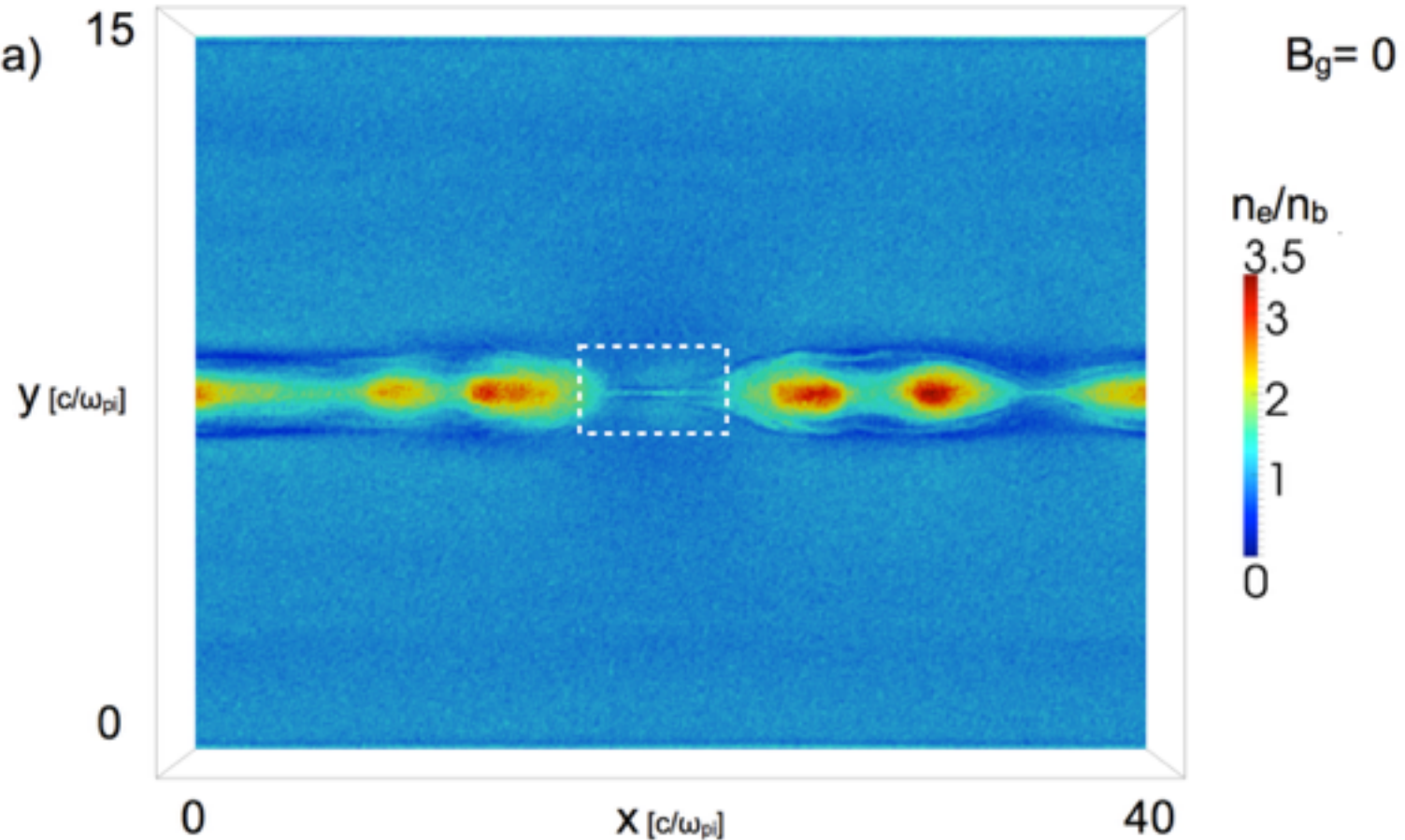
Electron density $n_e = 1.7 n_b$ (background density)

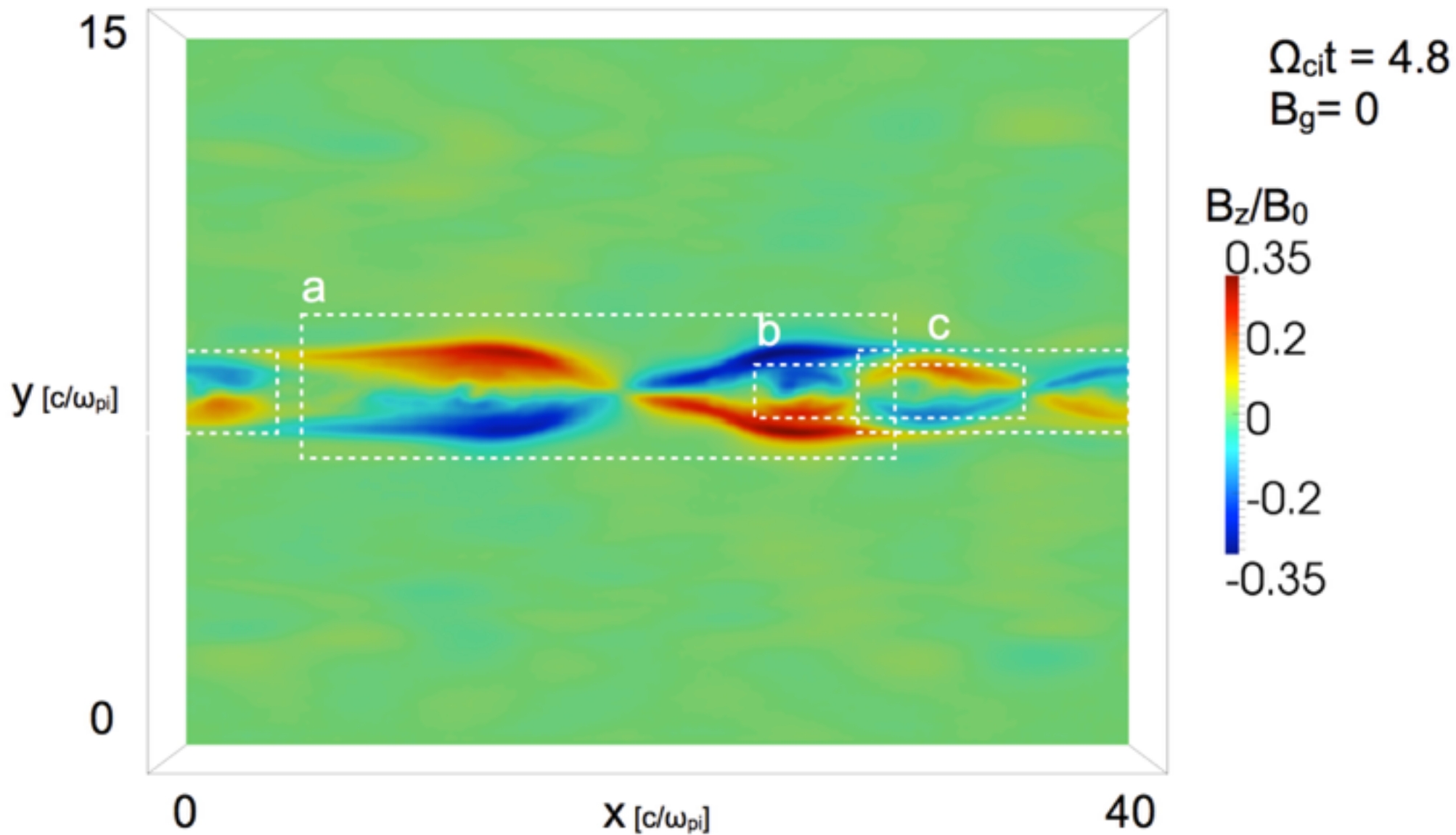
$$\Omega_{ci}t = 4.8$$



Electron density n_e contour plot on planes $z = L_z/2$ at $\Omega_{cit} = 4.8$

- Plasmoid enhanced density $\sim 3.5 \times n_b$.
- Formation of a **main reconnection region** in the middle of simulation box.



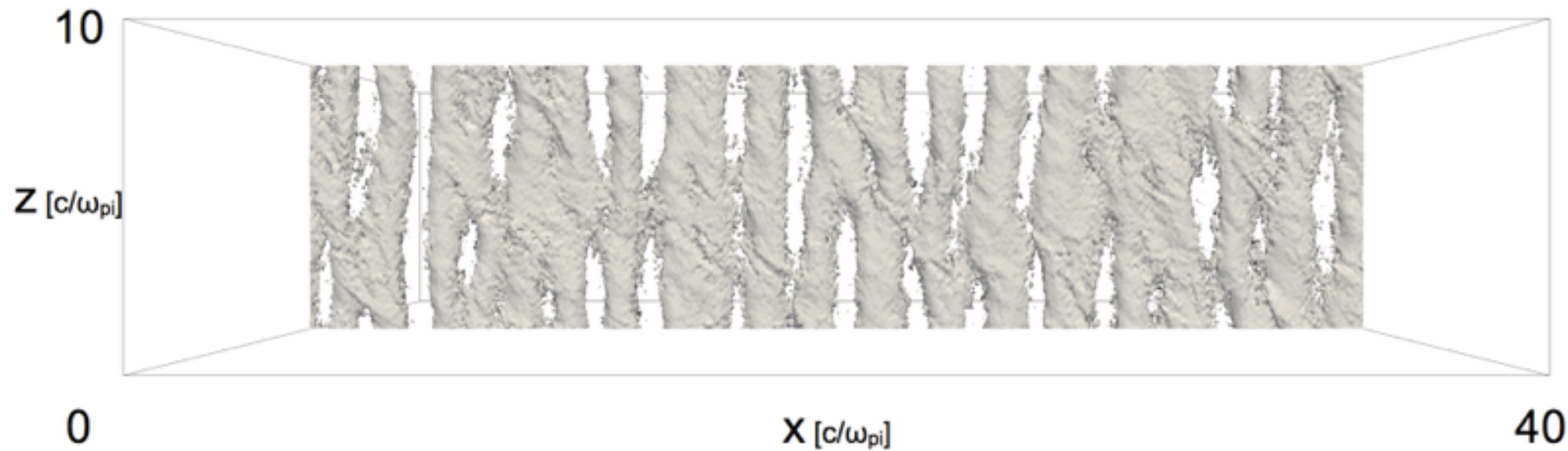


Hierarchical structure of Hall
magnetic field

Plasmoid chain dynamics in the guide field case

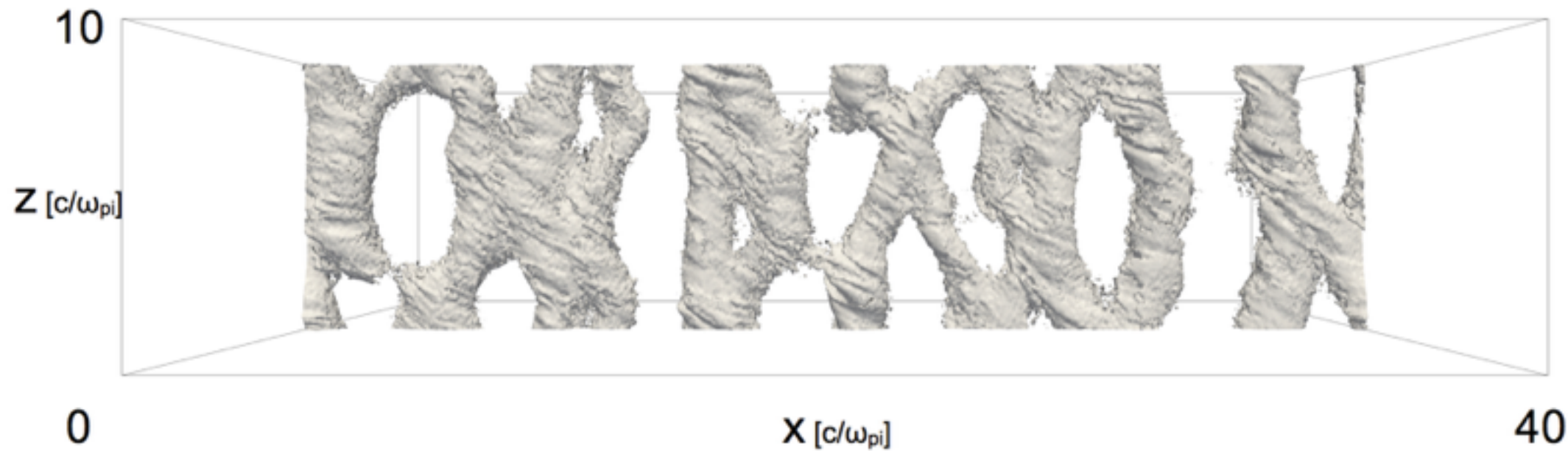
Electron density $n_e = 1.7 n_b$ (background density) $B_g = 1/3 B_0$

$$\Omega_{ci}t = 1.2$$



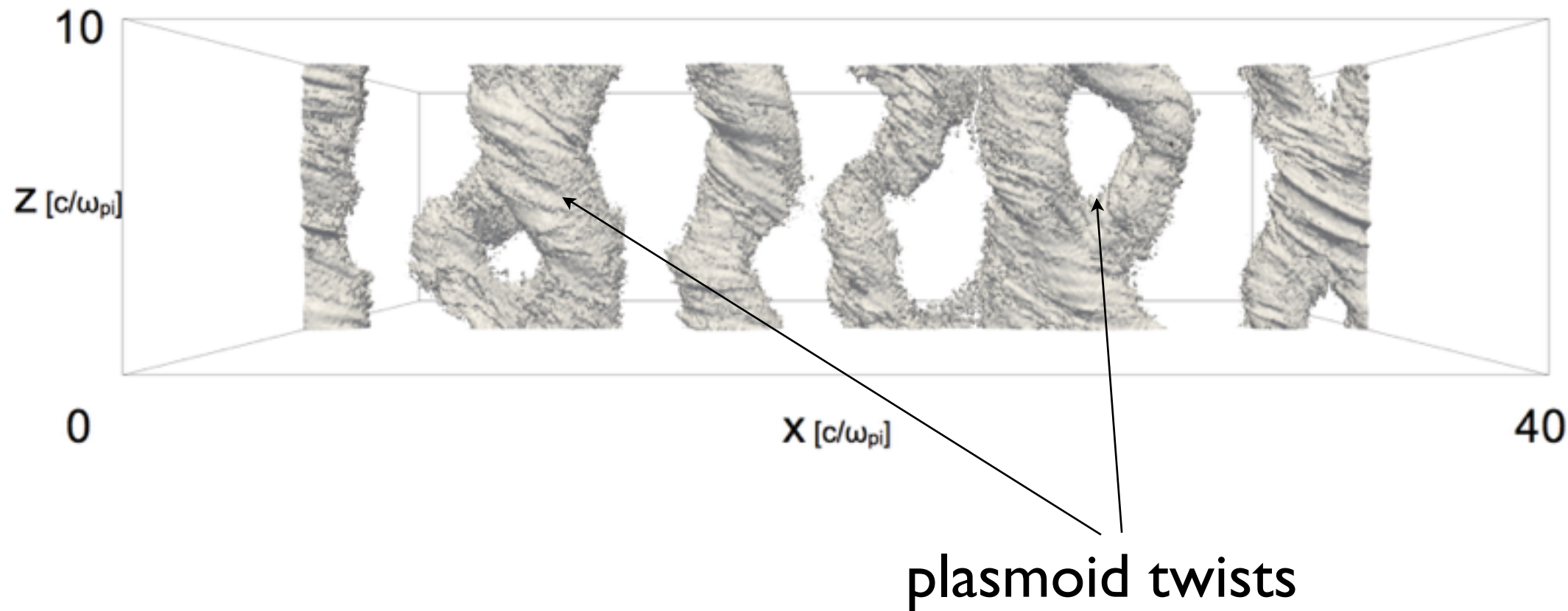
Electron density $n_e = 1.7 n_b$ (background density)

$$\Omega_{ci}t = 2.4$$



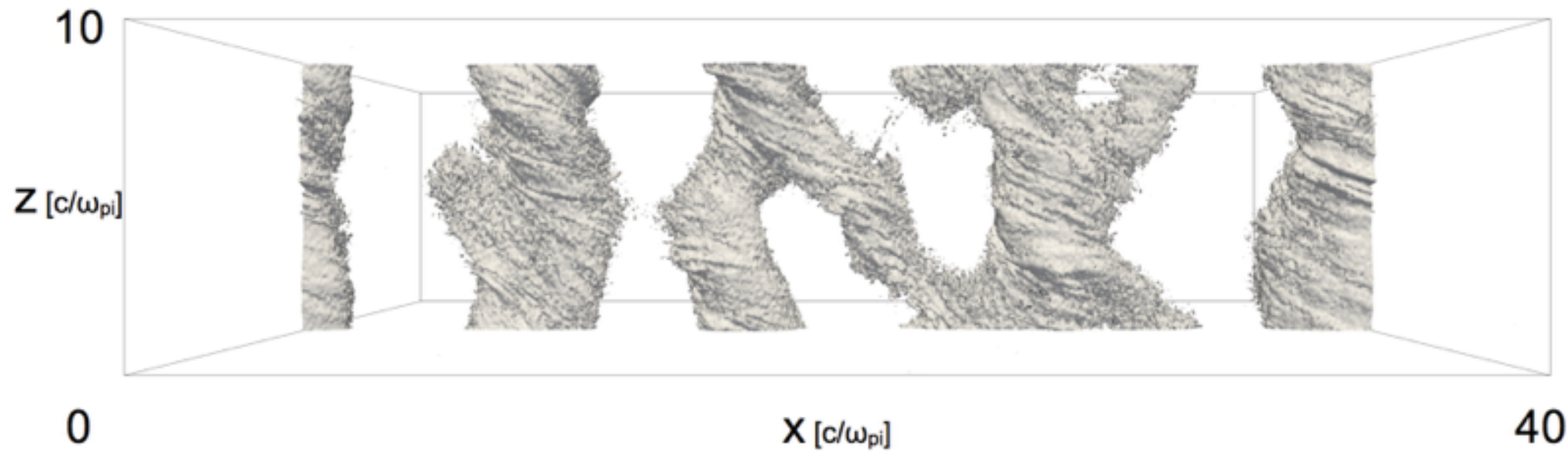
Electron density $n_e = 1.7 n_b$ (background density)

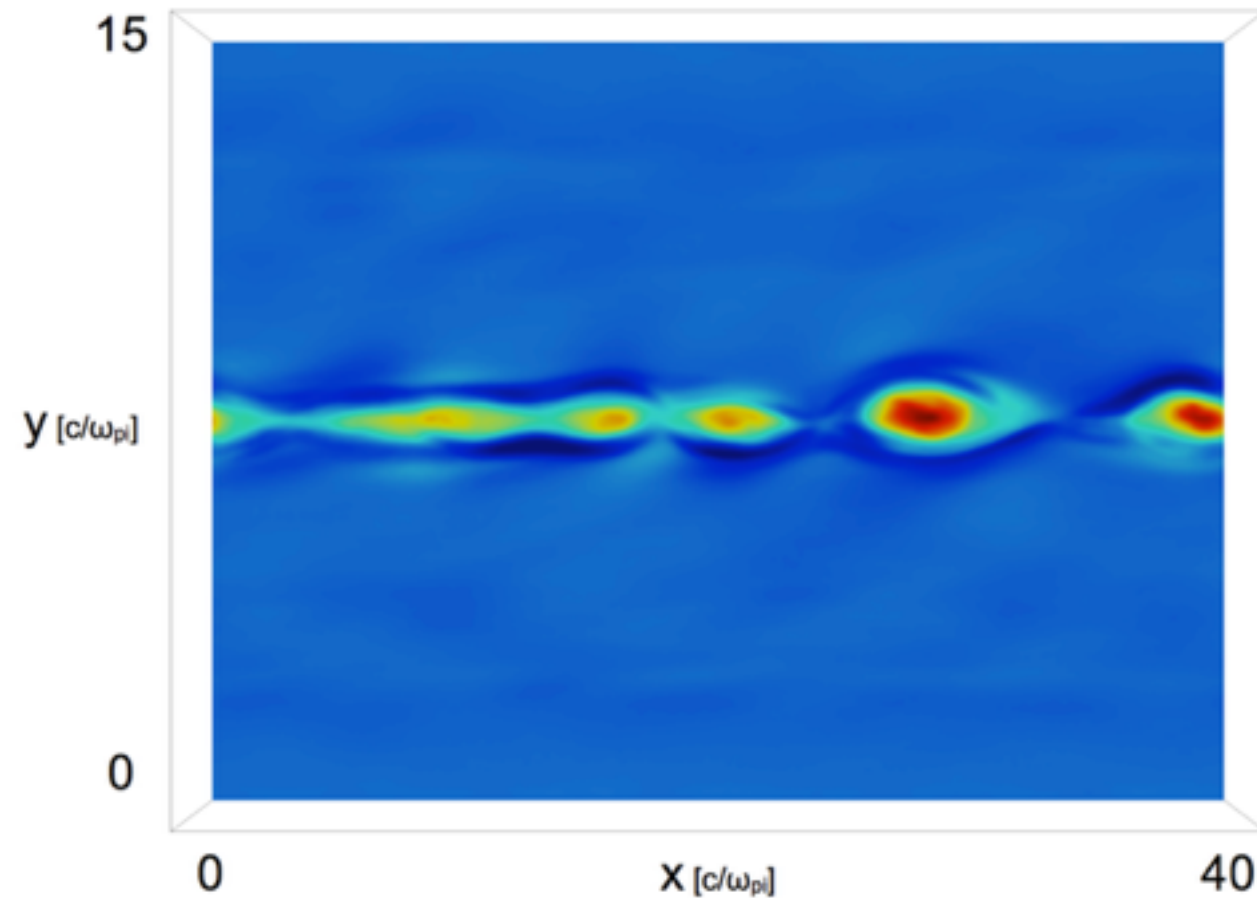
$$\Omega_{ci}t = 3.6$$



Electron density $n_e = 1.7 n_b$ (background density)

$$\Omega_{ci}t = 4.8$$





- With a guide field, B is characterized by unipolar core field

$$(B_z - B_g)/B_0$$

- Core magnetic field with maximum value equal to B_0 .
- Core magnetic field has the **same polarity of the guide field for all plasmoids** from the same current sheet.

The overall dynamics of plasmoids chain with and without a guide field is similar macroscopically (tearing, coalescence, kinking, lower hybrid waves). However, important differences are revealed:

- **Hierarchical structure of the plasmoid-dominated current sheets** is observed only in absence of a guide field. We believe that hierarchical structure is caused by Lower-Hybrid Drift instability thinning non uniformly the current sheet.
- **A strong core magnetic field** is observed only in presence of an initial guide field. This suggests that a core field arises only if a guide field is present.

Conclusions

- Presented 3D simulations of magnetic reconnection with iPIC3D starting from 3 different initial conditions to study different problems:
 - Antiparallel Harris equilibrium with perturbation to study instabilities of the reconnection fronts (kinetic interchange instability)
 - Harris equilibrium with guide field with perturbation to study instabilities along separatrices (presence of sub-cavities, electron MHD KHI, streaming instabilities).
 - Harris sheet non in equilibrium to study plasmoid chain dynamics in magnetotail condition (hierarchical structure of plasmoid-dominated current sheet in antiparallel configuration).